

To appear in *The Astronomical Journal*

Sulfur, Chlorine, and Argon Abundances in Planetary Nebulae. IV: Synthesis and the Sulfur Anomaly

R.B.C. Henry

*Department of Physics & Astronomy, University of Oklahoma, Norman, OK 73019;
henry@mail.nhn.ou.edu*

K.B. Kwitter

Department of Astronomy, Williams College, Williamstown, MA 01267; kkwitter@williams.edu

and

Bruce Balick

*Department of Astronomy, University of Washington, Box 351580, Seattle, WA 98195;
balick@astro.washington.edu*

ABSTRACT

We have compiled a large sample of O, Ne, S, Cl, and Ar abundances which have been determined for 85 galactic planetary nebulae in a consistent and homogeneous manner using spectra extending from 3600-9600 Å. Sulfur abundances have been computed using the near IR lines of [S III] $\lambda\lambda 9069, 9532$ along with [S III] temperatures. We find average values, expressed logarithmically with a standard deviation, of $\log(\text{S}/\text{O}) = -1.91 \pm .24$, $\log(\text{Cl}/\text{O}) = -3.52 \pm .16$, and $\log(\text{Ar}/\text{O}) = -2.29 \pm .18$, numbers consistent with previous studies of both planetary nebulae and H II regions. We also find a strong correlation between [O III] and [S III] temperatures among planetary nebulae. In analyzing abundances of Ne, S, Cl, and Ar with respect to O, we find a tight correlation for Ne-O, and loose correlations for Cl-O and Ar-O. All three trends appear to be colinear with observed correlations for H II regions. S and O also show a correlation but there is a definite offset from the behavior exhibited by H II regions and stars. We suggest that this S anomaly is most easily explained by the existence of S^{+3} , whose abundance must be inferred indirectly when only optical spectra are available, in amounts in excess of what is predicted by model-derived ionization correction factors. Finally for the disk PNe, abundances of O, Ne, S, Cl, and Ar all show gradients when plotted against galactocentric distance. The slopes are statistically indistinguishable from one another, a result which is consistent with the notion that the cosmic abundances of these elements evolve in lockstep.

Subject headings: ISM: abundances – planetary nebulae: general – stars: evolution

1. INTRODUCTION

The abundances and chemical histories of the elements sulfur, chlorine, and argon are important to study because this information provides valuable constraints on stellar evolution theory including yield predictions for massive stars. These three elements, the most abundant isotopes of which are ^{32}S , $^{35,37}\text{Cl}$, and ^{36}Ar , are produced during both hydrostatic and explosive oxygen burning (Pagel 1997; Woosley & Weaver 1995). In addition, they all produce prominent emission lines in gaseous nebulae, and so their abundances, particularly those of S and Ar, have been measured in numerous H II regions, supernova remnants, and planetary nebulae (PNe) in the Milky Way as well as in other galaxies. For objects located within the disk of a single galaxy abundance measurements can be combined with galactocentric distances and kinematics to provide valuable probes of galactic chemical evolution.

Planetary nebulae ostensibly serve as excellent probes of the interstellar abundances of S, Cl, and Ar at the time that their progenitor stars formed, generally more than a billion years in the past. PNe are produced when intermediate mass stars (IMS) with birth masses between 0.8 and 8 M_{\odot} shed a portion of their atmospheres late in the AGB stage of their evolution. This material is thought to have been enriched during prior episodes of dredge-up with products of core and shell H and He burning such as He, C, and N, consistent with the results of direct abundance measurements. Clearly, then, abundances of these three elements in PNe, while crucial for studying IMS nucleosynthesis, are not good gauges of the interstellar levels of these elements at the time of star formation. Likewise, it is also possible, though unconfirmed, that O in PNe is not a reliable gauge of its interstellar level either, since it may be enriched in PNe through the dredging up of He burning products containing large amounts of ^{16}O or depleted through ON cycling during H burning. In addition, the Ne abundance may be enhanced in PNe through the conversion of ^{14}N to ^{22}Ne . So, the PN abundances of O and Ne, in addition to those of He, C, and N may prove to be unreliable measures of interstellar levels at the time the progenitor stars were formed. At the same time, the abundances of S, Cl, and Ar are presumed to remain unchanged from their levels in the ISM at the time and location of star formation; there is currently no theoretical prediction to the contrary.

Early PN abundance work on S, Cl, and Ar includes the optical studies by Barker (1978a), in which he measured S abundances in 37 galactic PNe using spectroscopic measurements which included the important nebular lines of [S III] $\lambda\lambda 9069, 9532$ along with [S II] $\lambda\lambda 6716, 6731$. This paper was followed up by a closer study of 20 of those same objects (Barker 1978b) and a third paper on three halo PNe (BB-1, K648, and H4-1) (Barker 1983), using similar techniques. Barker (1980) also reported on observations of [Ar III] $\lambda 7135$ in the same three halo PNe. In the end, he concluded that the S abundance in most PNe is roughly solar but that in the halo objects both S and Ar abundances are markedly lower, in qualitative agreement with Hawley & Miller’s (1978) S measurement in H4-1 and later confirmed by Barker & Cudworth (1984) in DdDm-1. Other confirmations of low S and Ar in halo PNe were supplied by Torres-Peimbert & Peimbert (1979), and Peña, Torres-Peimbert, & Ruiz (1991). Since Barker also found the O and Ne abundances

to be both less depleted with respect to solar and uncorrelated with S and Ar, he suggested that the former two elements may be enhanced by nuclear reactions in the PN progenitors through the nuclear processes discussed above, making S and Ar perhaps a better gauge of progenitor composition. Two large optical studies by Aller & Czyzak (1983) and Aller & Keyes (1987) of 41 and 51 galactic PNe, respectively, provided S, Cl, and Ar abundances for many more objects with the suggestion that on the average these three elements tend to have subsolar abundances.

While optical spectra permit direct observation of S^+ and S^{+2} through the measurement of [S II] $\lambda\lambda 6716, 6731$ and either [S III] $\lambda 6312$ or the two near IR (hereafter NIR) [S III] lines at $\lambda\lambda 9069, 9532$, photoionization models suggest that S^{+3} , which has a strong emission line in the infrared but none in the optical, may also be an abundant ion in PNe. In work limited to the optical, then, the abundance of S^{+3} is customarily accounted for through the use of an ionization correction factor (ICF). The sulfur ICF is discussed in detail in Kwitter & Henry (2001; Paper I) as well as in §4.2.5 below.

Observation of the S^{+3} emission line at $10.5\mu\text{m}$ in the infrared allows direct measurement of the S^{+3} abundance. This abundance, when added to the optically observed S^+ and S^{+2} abundances¹, gives total S, eliminating the need for an ICF. Such an approach was pioneered by Dinerstein in her thesis (Dinerstein 1980a) and in Dinerstein (1980b), in which she measured the [S IV] $10.5\mu\text{m}$ emission in 12 galactic PNe. Combining these measurements with optical data obtained by Lester, Dinerstein, & Rank (1979), abundances of the three S ions were computed and S/H ratios established. Their results indicated that S/H in their sample objects was roughly solar. Then Garnett & Lacy (1993) employed similar IR techniques to study S in two halo PNe, K648 and BB-1, and were able to reconfirm Barker’s low S/O values in these objects. Very recently Dinerstein et al. (2003) have extended their work to include IR observations of two halo PNe, DdDm-1 and H4-1. They also find low S/O ratios and suggest, as Barker and Garnett & Lacy had, that O enrichment had occurred in these low metallicity objects, an idea also proposed by Péquignot et al. (2000) following the analysis of two PNe of roughly half-solar metallicity in the Sagittarius dwarf galaxy. Finally, IR observations were also used by Beck et al. (1981) to infer S and Ar abundances for 18 galactic PNe. This group found some deviation from the expected lockstep behavior of S and Ar.

Since the late 1980s numerous additional optical studies of S, Cl, and Ar in PNe have appeared. These include a survey of 14 Galactic objects by Gutiérrez-Moreno & Moreno (1988), 43 Galactic objects by Freitas Pacheco et al. (1991; 1992), 15 Galactic PNe by Costa et al. (1996), 23 LMC PNe by Freitas Pacheco et al. (1993a,b), 80 Galactic objects by Kingsburgh & Barlow (1994; hereafter KB), and 15 PNe (twelve Galactic and three in the LMC) by Tsamis et al. (2003). Howard, Henry, & McCartney (1997) carried out a detailed photoionization analysis of nine halo PNe and included S and Ar in their list of elements. Finally, Maciel & Köppen (1994), Maciel & Chiappini (1994), and Maciel & Quireza (1999) published large compilations of S, Cl, and Ar abundances and applied

¹Care must be taken to ensure that the nebular regions observed and the aperture sizes utilized in the optical and IR are the same, or that differences are accounted for as fully as possible.

the data to the study of galactic chemical gradients. The general conclusion that can be gleaned from the above studies is that S/O is often found to be less than either the solar or H II region value, while Cl/O and Ar/O appear to be consistent with these levels².

Despite the large amount of S, Cl, and Ar abundance information already available for PNe, we undertook a new study of these elements five years ago, because we were aware that most previous S studies had been based on the [S III] auroral line at 6312 Å, although potentially better abundance information could be derived using the strong lines of [S III] $\lambda\lambda$ 9069,9532. In addition, we were intrigued by the implication, already noticed by Freitas Pacheco (1993), that significant amounts of S, Cl, and Ar may be produced by Type Ia supernovae (Nomoto et al. 1997), and thus we wanted to see if, in the possession of consistently determined data for a large PN sample, along with published stellar yields, we could test the hypothesis that SNIa make noticeable contributions to the cosmic buildup of these three elements.

The current paper is the fifth one in a series dealing with an extended project in which the abundances of S, Cl, and Ar (in addition to He, N, O, and Ne) have been determined for 85 galactic PNe. In the previous four papers, spectral data and abundance calculations were presented for subsets of this sample: Kwitter & Henry (2001; Paper I), Milingo, Kwitter, & Henry (2002; Paper IIa), Milingo, Henry, & Kwitter (2002; Paper IIb), and Kwitter, Henry, & Milingo (2003; Paper III). The present paper attempts to collate all of the abundances previously reported and to compare the large sample with analogous information from other PN samples as well as H II regions in order to identify and comment upon trends. In section 2, we briefly discuss the nature of our PN sample, while in section 3 we present results of our study pertaining to electron temperatures. Section 4 contains an extensive discussion of our abundance results, while we present our results pertaining to Galactic chemical gradients in section 5. Our conclusions are presented in section 6. Future papers will address questions related to population, morphological type, and abundances as well as the potential impact of Type Ia supernovae on the cosmic buildup of S, Cl, and Ar.

2. THE DATA

The sample of PNe which is the subject of this paper comprises 85 Galactic objects³. Table 1 contains the common name of each object in the first column along with the Peimbert type in the second column. By type our sample includes 12 Type Is, 69 Type IIs, and 4 halo or Type IVs. These types, originated by Peimbert (1978), classify PNe primarily according to chemical composition, a proxy for their progenitors' galactic population characteristics. Type Is are those with

²Here, the solar value for $12+\log(\text{O}/\text{H})$ has been taken to be 8.69, as published by Allende Prieto, Lambert, & Asplund (2001).

³Note that NGC 2242 was part of the original sample, but we have eliminated it from consideration in this paper, as its extremely high excitation level makes the derived abundances uncertain (Paper III).

enhanced nitrogen (and often, helium) abundances, assumed to result from younger, more massive progenitors; Type IIs are intermediate population with less enhancement; Type IIIs have similar abundances to Type IIs, but in addition have higher peculiar velocities; and Type IVs are halo PNe.

The original Type I classification included both enhanced He/H and N/O. In this work, we follow the discussion found in KB, who use only the nitrogen abundance as a discriminant. They set the minimum nitrogen abundance for Type I classification in a given galaxy equal to the sum of the carbon plus nitrogen abundances of H II regions in that galaxy. Assignment of Type I status thus requires that nitrogen must have been produced by conversion of carbon in the envelope of the progenitor star (so-called "hot-bottom burning"). KB calculated the equivalent minimum N/O ratio for Type I PNe in the Galaxy to be 0.8. Using more recent abundance measurements for the Orion Nebula (Esteban et al. 1998) and for the sun (Grevesse & Sauval 1998), we derive a somewhat lower minimum N/O ratio of 0.65, which we have applied here.

Our sample was purposely chosen to contain a large majority of Type II objects. These objects are ideally suited for probing the interstellar medium, as they are known to be disk objects with relatively lower progenitor masses than the Type Is, and hence they are less likely to be self-contaminated with nucleosynthetic products. An important selection goal was to produce a program list which collectively spanned a large range in galactocentric distance. In this respect, our objects range from 2-17 kpc.

Spectrophotometric data covering the region between 3600 and 9600 Å were obtained for each of our program objects using either the 2.1 m telescope and Goldcam spectrograph at KPNO or the 1.5 m telescope and the Cassegrain spectrograph at CTIO between 1996 May and 1999 July. The data were reduced, dereddened, and measured using standard IRAF routines. Abundances were uniformly calculated using the program and procedure discussed in detail in Paper I. Specific references for the atomic data used in the abundance calculations are listed in Table 4 of that paper along with an extended discussion of the ionization correction factors employed.

Above all, our goal has been to produce a large homogeneous sample of PN abundances starting with state of the art optical spectrophotometry and using up-to-date atomic data consistently throughout our study as much as possible. Researchers can view and manipulate the reduced spectra for each of our objects at our *Gallery of Planetary Nebula Spectra* website⁴. Additional information as well as links to images of each object and a set of student lab exercises using these data will be found there. Questions regarding the website or the original data or should be addressed to K.B. Kwitter (kkwitter@williams.edu).

⁴<http://cf.williams.edu/public/nebulae/index.html>

3. ELECTRON TEMPERATURES

Electron temperatures and densities for our sample objects are compiled in Table 2. The references for these values are identical to those listed in the last column of Table 1. Due to an oversight in earlier papers, effects of density were not accounted for in the determination of the [N II] temperature in those objects where the density exceeds 5000 cm^{-3} . This problem has been addressed, and the updated values for the relevant objects now appear in Table 2. Fig. 1 shows five electron temperatures, [O III], [N II], [O II], [S II], and [S III] plotted together in various combinations for our objects, where temperatures are in units of 10^4 K , and the diagonal lines show one-to-one relations⁵. Each panel is labeled to show the specific temperatures being plotted, in Y v. X format, along with a representative error bar of $\pm 1000 \text{ K}$.

In the left panels of Fig. 1 there are suggestions of correlations between the [S II] and [O II] temperatures (top left), and between each of these and the [N II] temperature (middle and lower left), although the scatter is large in each case. The ionization structure of model nebulae indicates that these three ions should coexist spatially, and so it is somewhat surprising that the correlations in the left panels involving these temperatures are not greater. In the right panels we have plotted the [N II], [O II] and [S III] temperatures as a function of the [O III] temperature. In the upper panel, there is a suggestion of a positive correlation between the [N II] and [O III] temperatures below 10,000 K for both temperatures, but above that level we see a large amount of scatter.

The most interesting result in Fig. 1 is the relation between the [O III] and [S III] temperatures shown in the lower right panel, a relation previously seen in H II region studies by Garnett (1992), Vermeij & van der Hulst (2002), and Kennicutt, Bresolin, & Garnett (2003; hereafter KBG). Systematically, we find [S III] temperatures are greater than [O III] temperatures in PNe, and the difference seems to grow with [O III] temperature. A linear fit to the trend is shown in the figure as a solid bold line with a correlation coefficient of 0.79 and an equation of the form

$$T_{[\text{S III}]} = -0.039(\pm 0.11) + 1.20(\pm 0.11) \times T_{[\text{O III}]}, \quad (1)$$

where both temperatures are in units of 10^4 K . We also show for comparison purposes the analogous form derived by Garnett (1992), $T_{[\text{S III}]} = 0.17 + 0.82T_{[\text{O III}]}$, which he derived from a photoionization model study of H II regions. Clearly, for PNe the latter expression underestimates the [S III] temperature for a given [O III] temperature, but this may be related to general density differences between PNe and H II regions, since the greater values seen in the former may result in a different thermal structure in these objects. Our expression can be used to obtain [S III] temperatures from [O III] temperatures with an uncertainty of $\sim 1000 \text{ K}$. Researchers may find this relation particularly useful for obtaining S^{+2} abundances when the lack of [S III] nebular lines due to spectral limitations prohibits the direct determination of the [S III] temperature.

⁵The specific lines used for temperature determinations are as follows. [O III]: nebular, $\lambda\lambda 4959, 5007$, auroral, $\lambda 4363$; [N II]: nebular, $\lambda\lambda 6548, 6584$, auroral, $\lambda 5755$; [S III]: nebular, $\lambda\lambda 9069, 9532$, auroral, $\lambda 6312$; [O II]: nebular, $\lambda\lambda 3726, 3729$, auroral, $\lambda 7325$ (quartet); [S II], nebular, $\lambda\lambda 6716, 6731$, auroral, $\lambda 4072$ (quartet).

There is noticeable scatter in all of the panels of Fig. 1. In some cases, the cause could be that the two relevant ions do not exist in the same region of the nebula. For example, photoionization models suggest that O^+ and N^+ do not coexist spatially with O^{+2} . Thus we might expect scatter when their temperatures are plotted against the [O III] temperature. Additional factors which lead to scatter in [O II] temperatures were explored by KBG and include radiative transfer effects and shock heating. Additional sources of scatter may be uncertainties in line intensities and reddening. Finally, variations in density and temperature along the line of sight could introduce scatter. In the low density limit, observed line intensities are line-of-sight integrations of the product of density and excitation rate, where the latter has a maximum value at a specific optimum temperature which generally is not the same for both the nebular and auroral lines comprising the temperature diagnostic. This means that the regions of the nebula responsible for the bulk of the emission may be different for the two line types, and thus may be weighted by different densities. In this way, an observed nebular to auroral line strength ratio may not imply the true representative temperature, i.e. the presence of such inhomogeneities may cause the line ratios used in determining temperatures to be skewed up or down.

4. ABUNDANCES

4.1. General Results

A complete summary of abundances for He/H, O/H, Ne/O, S/O, Cl/O, Ar/O, and N/O⁶ for our 85 survey objects is provided in Table 1. The first column gives the object name and the second column the Peimbert type according to the criterion described in §2 ($N/O \geq 0.65$). We also provide an estimate of the galactocentric distance of each object in kiloparsecs, where the distances were determined using basic information in the references cited in the relevant table footnote. The abundances were derived from spectra reported and analyzed in the preceding papers in this series; information in the last column of the table gives the reference source for the abundances of a particular object. Also, we have included 10 objects in Table 1 for which line strengths and some abundance results were reported in an earlier series of papers. We recalculated all abundances for these 10 objects, including those of S, Cl, and Ar which were excluded in the original determinations, and include them in Table 1. A tabulation of ionic abundances, electron densities and temperatures for these objects is provided in Appendix A. Finally, the last four rows of Table 1 give averages for sample subsets as well as for the entire group of objects. Uncertainties in elemental abundances given in the table are ultimately derived from line strength uncertainties and their effects on ionic abundances. Uncertainties in the latter were added in quadrature to produce the elemental abundance final uncertainty. Readers are referred to the earlier papers in this series for a detailed discussion of our abundance-determining methods.

⁶The N/O ratios for those objects for which temperatures have been corrected for density effects (see §3) have likewise been updated and included in this table.

Table 3 provides a comparison of our abundance ratio averages for S/O, Cl/O, and Ar/O with those found in numerous other studies of PNe and H II regions, as well as values observed in the Sun (Grevesse & Sauval 1998). Column 1 gives the source reference, while column 5 provides comments pertaining to each sample. Values given in columns 3, 4, and 5 are logarithms of arithmetic averages. In the case of PNe, the number of sample objects contributing to an average value is given in parentheses. It should be pointed out that our PN study is the only one on the list that utilized the NIR lines of [S III]; in all of the other cases S⁺² abundance computations were based on the $\lambda 6312$ line.

The three ratios considered in Table 3 are of interest in that they involve elements whose abundances ostensibly vary in lockstep, according to standard nucleosynthesis theory. Each ratio, then, should provide a key check on the relative stellar yields for the two elements, and they should show consistency between PNe and H II regions, since their values in the former should not be altered by nuclear processes in the progenitor star but reflect interstellar values at the time of star formation. Indeed the average abundance ratios for Cl/O, and Ar/O are very consistent between all of the PNe and H II region samples as well as in the Sun, in accord with the above ideas. *However, based upon the numerous PN studies included in Table 3, S/O seems to be less in PNe than in H II regions and the Sun.* Our results are no exception.

The four panels in Fig. 2 show separately the correlations between Ne, S, Cl, and Ar, versus O for both our sample objects (open circles) and H II regions (filled symbols). The bold, solid line in each panel shows a least squares linear fit to the data, where the values for slope, intercept, correlation coefficient and number of included sample objects are listed in Table 4. In three panels the H II region abundances reported by KBG for M101 are shown with filled circles. We include their data for comparison, because it is characterized by high signal-to-noise and, in the case of sulfur, they derive S⁺² abundances using the NIR lines, as we did.

We note in Table 4 that the correlation coefficient for Ne is especially high, and the relation between Ne and O found here is remarkably similar to the one found by Henry (1989) in which the intercept was $-2.14(\pm 0.04)$, the slope was $1.16(\pm 0.33)$, and the correlation coefficient was 0.91. The current data simply reconfirm the tight relation between these two elements. In addition, we see that the M101 H II region data fall very nicely along the linear fit for the PNe, in strong support of the ideas that these elements are forged together, vary in lockstep, and that PN measurements of these elements measure interstellar values, with no discernable contamination from or depletion by the progenitor star.

In the cases of Cl and Ar, however, the scatter in Fig. 2 is observed to be slightly greater than for Ne, especially for PNe. Generally speaking, these elements are products of both hydrostatic and explosive oxygen burning and require several alpha reactions to produce them, perhaps making their production rates more vulnerable to local conditions. In addition, the line strengths required to measure their abundances are generally weaker than those for O, Ne, and S. Thus, the larger scatter is anticipated. Note also that the M101 Ar abundances appear to be slightly larger systematically

compared to the PN Ar abundances.

We have identified several outliers in three of the panels in Fig. 2. It is interesting to note that three of these objects, BB1, H4-1, and K648, are halo PNe. Howard et al. (1997) found that abundances in halo PNe often exhibited inconsistent behavior with respect to disk objects, a pattern also seen in abundance studies of halo stars (Snedden & Cowan 2003; Truran et al. 2002).

But by far the most intriguing result in Fig. 2 is that PNe behave differently from the H II regions of M101 in the S-O plane. In the Introduction, we briefly discussed a few cases of individual low-metallicity PNe in which the S/O ratio was found to be subsolar. Specifically, papers by Barker (1983), Howard, Henry, & McCartney (1997), Péquignot et al. (2000), and Dinerstein et al. (2003) make note of this anomaly. Yet here we find the problem to be pandemic, stretching broadly across the metallicity range for a large sample of objects. Recall that in our discussion of Table 3 we pointed out that average S/O values in PN samples tend to be less than in H II regions. In Fig. 2 we see just how extensive this pattern is. Interestingly, this general trend has not been noticed before, perhaps because a broad, detailed intercomparison among PNe and H II regions and the Sun for these elements has not previously been made.

Assuming that H II region S and O abundances represent the true interstellar values⁷, then is the depressed S/O value in PNe relative to H II regions produced by low S abundances or high O abundances? The suggestion has been made in a few of the papers cited above that the anomalously low S/O in a few metal-poor PNe might be the result of O synthesis as the result of He burning in the progenitor star. However, the positions of PNe in the Ne-O plane seem to argue otherwise. For example, the PNe and H II regions fall along the same line in the Ne-O plane (upper left panel), suggesting that if O enrichment is indeed occurring as proposed, then so too is Ne enrichment and in the same proportion, since otherwise, the PNe would be offset to the right of the H II region track. But since it is unlikely, due to temperature constraints, that excess ²⁰Ne is produced by the same He burning that allegedly produces the O, then excess Ne would have to come from ²²Ne production from ¹⁴N, and it is difficult to imagine that this channel would operate at just the proper rate necessary to maintain the PN positions on the Ne-O track in Fig. 2. Finally, if the S-O anomaly in PNe is the result of problems inherent in the abundance determinations, again the tight Ne-O correlation for PNe suggests that the culprit must be S, not O. Therefore, we conclude that the S-O anomaly in the upper right panel is most likely related to S abundances, not O abundances, and is therefore a S anomaly. In the following subsection we proceed with that assumption in an

⁷Chemical evolution theory predicts that a unique, spatially independent relation exists between oxygen and sulfur (and other alpha elements) production over the entire metallicity range such that the two elements evolve in lockstep. This situation arises because both elements are produced predominantly in massive stars. The observed correlation between S/H and O/H abundances in H II regions residing in various galaxies with different rates of evolution and age-metallicity relations (§4.2) strongly supports this idea observationally. For our PN observations of low S/O to be an effect of chemical evolution would seem to require that the interstellar gas which formed these PNe was processed under vastly different conditions than was the gas which formed the H II regions. e.g. a much different stellar initial mass function. For the time being we rule out this possibility.

effort to understand the origin of the anomaly.

4.2. The Sulfur Abundance Anomaly

To study the S abundance anomaly in more detail, we add other H II region samples, as well as stellar samples, to the S-O plot of Fig. 2 and display the result by itself in enlarged format in Fig. 3a. Noting that the combined H II region and stellar data form a rather narrow, linear track extending over roughly 1.5 dex along both axes, we make the following points: 1) Compared with H II regions and stars, PN sulfur abundances are systematically lower, particularly at subsolar oxygen levels; and 2) PNe exhibit a large amount of scatter in the S-O plane, while H II regions show a relatively tight correlation. To make the point that the S anomaly is investigator-independent, we plot KB’s abundances for their large sample of PNe, derived using the $\lambda 6312$ line, in Fig. 3b along with the same H II region-stellar comparison data shown in Fig. 3a. KB’s abundances are taken from their Table 13. Clearly, the anomaly is not new, just heretofore unrecognized. Assuming that the track defined by the H II region data in Fig. 3a defines the true interstellar relation between S and O, the sulfur anomaly refers to the situation in which many PNe appear to have a deficient amount of S relative to the interstellar value associated with their O/H ratio. We now briefly explore possible explanations for the sulfur anomaly.

If our sample of PNe are drawn from a population which is distinct from H II regions, then the abundance of one element with respect to another can be much different, perhaps due to mixing of star-forming gas. Witness the numerous examples common in the literature today in which abundance patterns in metal poor systems exhibit considerably more scatter and incoherence than do patterns associated with disk systems (McWilliam 1997). A detailed study of our sample with regard to population is beyond the scope of this paper. However, simple comparisons of S/O ratios of our PNe with their galactocentric distances and heights above the plane currently reveal no systematic behavior. At the same time, we expect that our sample of objects is relatively homogeneous, in that we purposely chose a group of objects the vast majority of which are Peimbert Type II PNe, meaning that they currently are part of the disk population. So, we do not expect population-related factors to be the cause of the S anomaly.

Another possibility is that sulfur is depleted onto dust in many PNe. However, Savage & Sembach (1996) found that sulfur is not greatly refractory and does not form dust readily, so this explanation for the anomaly seems unlikely. Likewise, nucleosynthesis arguments appear untenable. In Fig. 2 we saw that Ne, Cl, and Ar in both H II regions and PNe follow a near lockstep behavior with O, and it seems likely from a theoretical point of view that S would behave in a similar way.

The most likely cause of the S anomaly, then, is some factor related to the determination of the S abundance itself. In an effort to spot potential fundamental problems in our calculations, we compared our S abundances with those of KB for the PNe appearing in both samples and found satisfactory agreement between the two sets of values. Along the same lines, we used our methods

to calculate S abundances using KBG’s H II region data and found very close agreement with their published abundances. Finally, we recalculated all of our S^{+2} abundances using the [S III] $\lambda 6312$ line rather than the NIR lines. This method produced abundances which were slightly higher systematically⁸, although the offset was entirely insufficient for explaining the sulfur anomaly.

Next, in an attempt to independently confirm the S anomaly using a different abundance technique, we calculated photoionization models for IC 4593, Hu2-1, and NGC 3242, three PNe whose S abundances fall significantly below the S-O relation defined by H II regions. We chose these three particular objects because their C abundances have been measured (Henry, Kwitter, & Bates 2000), an important factor, since C can be a significant coolant and thus a parameter that needs to be constrained if possible. We used the photoionization code CLOUDY version 90.4 (Ferland 1996). Important observationally constrained input parameters were the central star temperature, and the nebular $H\beta$ luminosity, density, radius, and chemical composition. We proceeded by setting the model parameters, including abundances, equal to the observed ones, calculating a model, comparing output line strengths with the observations, making changes to the input parameters, and continuing to iterate until model and observed line strengths matched closely. We assumed a blackbody shape for the stellar spectrum along with a constant density spherical nebula.

Table 5 lists the observed and model-predicted line strengths by object in the upper part of the table, while in the lower section the observed and model-input parameter values are provided. Observed quantities were taken from sources detailed in the table footnotes. The first eight lines of model parameters give abundance information, followed by the central star’s effective temperature, the nebular $H\beta$ luminosity, electron density, radius, and filling factor.

The two important points to recognize in Table 5 are that the model output line strengths agree closely with the observations for all three objects, and that the observed abundances, i.e. those in Table 1, agree well with the ones necessary in the model to produce the line strength agreement. In particular the model O and S abundances agree with their observed counterparts to within about 0.1 dex. To emphasize this point, the positions of the models in S-O abundance space are shown in Fig. 3a with large stars and labelled by object name. Note that the model and observed positions for IC 4593 and NGC 3242 are offset slightly (the two lines point to the model and the observed data point) while for Hu2-1 the model and observed points are nearly on top of one another. We conclude that photoionization models, which are heavily constrained by numerous observed quantities, imply S and O abundances which agree closely with those already inferred and confirm the existence of the S anomaly in these three objects. Therefore, if there is a problem with our analysis procedure, then the trouble extends to the models as well. Such a problem is likely to be related to our lack of understanding of the details of the ionization structure of objects exhibiting the S anomaly. *We propose that the probable cause of the S anomaly is the failure to adequately measure indirectly, through the use of an ICF, all of the S^{+3} present in those nebulae which display a large S deficit.* In other words, common forms of the sulfur ICF must be

⁸This was most likely because [N II] temperatures were used in place of the generally higher [S III] temperatures.

flawed.

Any choice of ICF for sulfur can, in principle, be checked empirically by comparing the S^{+3} abundances it implies⁹ with directly observed values in objects where the [S IV] $10.5\mu\text{m}$ strength has been measured. Table 6 provides such a comparison for 14 of our objects for which IR data are available. In columns 2 and 3 we give the S^{+3}/H^+ abundance ratio as inferred from our original ICF and from the IR data, respectively, while column 4 gives the ratio of these two quantities. The first number in the last column indicates the source for the column 2 abundances, while the second number does the same for column 3. For reference 6, the ratios quoted here were actually computed using our ionic abundance routines along with Dinerstein’s (1980b) original line strengths for [S IV]. We employed the [S IV] collision strengths of Tayal (2000). Numbers in column 4 indicate a general tendency for our ICF method to underestimate the S^{+3} contribution to the S abundance, a trend that can be seen graphically in Fig. 4, where we plot S^{+3} abundances derived from the IR against the same parameter inferred from the ICF. In Table 6 the average of the ICF-to-IR values between 0 and 1 is .55 or -.26 dex. Interestingly, the latter offset is consistent with the amount by which objects in Fig. 3a tend to fall below the H II regions, consistent with our contention that our ICF undercorrects for S^{+3} . (As a caveat, we point out that positions and aperture sizes employed for the optical and IR observations of each PN do not necessarily coincide for the 14 objects analyzed here, so the results of this comparison are only tentative. To improve on this analysis idea, therefore, it will be necessary to sample many more PNe, using consistent aperture sizes and positioning.)

Finally, we define the sulfur deficit as the magnitude of the vertical offset of a PN from the H II region track at a specific metallicity (O/H) in the S-O plane and assume that it represents the amount of S^{+3} which is unaccounted for through our methods. We have estimated the sulfur deficit for each object in our sample by employing a least squares fit to the H II region data in Fig. 3a¹⁰. Upon plotting the deficit values against various other quantities, an interesting correlation with O^{+2}/O abundance ratios was found. This relation is displayed in Fig. 5, where the sulfur deficit is plotted on the vertical axis in units of $10^5 S^{+3}/H^+$. Note that PNe with greater sulfur deficits are positioned higher in the plot. There is a slight tendency for the S deficit to be higher in objects where the O^{+2}/O ratio is low. The interpretation of this, however, is unclear, since O^{+2}/O can be small either because of high or low excitation, and likewise because of matter or radiation boundedness. But whatever the explanation, more S^{+3} than expected tends to be present when this ratio is low. The sulfur deficit could arise if a process contributing to the ionization balance between S^{+3} and S^{+2} is unaccounted for. Candidates include a higher than expected S^{+2} photoionization cross-section, a low rate of recombination for S^{+3} , peculiarities in the central star spectrum which selectively force the ionization equilibrium upwards, or highly matter-bounded gas dominated by S^{+3} . We emphasize that these possibilities need not be inconsistent with the fact that H II regions do not exhibit the S anomaly, since in the latter objects the excitation level is much lower and the

⁹ $S^{+3}=(S^++S^{+2}) \times (\text{ICF}-1)$

¹⁰ $12 + \log(S/H)_{\text{H II}} = -3.37 + 1.22[12 + \log(O/H)]$

abundance of S^{+3} is expected to be extremely low. Any of the above possibilities would not likely be evident in the observed ion abundances.

5. GALACTIC ABUNDANCE GRADIENTS

Figures 6a-e show the abundances of O, Ne, S, Cl, and Ar, expressed as $12+\log(X/H)$, as functions of galactocentric distance in kiloparsecs in the galactic disk as tracked by our PNe. Our data, taken from Table 1, are shown as open circles in each case. Fig. 6a shows our results for oxygen along with the H II region and stellar data taken from the literature and detailed in the figure captions. Figures 6b-e give analogous results for Ne, S, Cl, and Ar, respectively. Data for the halo PNe K648, DdDm-1, BB1, and H4-1 are not included in these plots. The solar value indicated in each plot by a large S is the photospheric value of Allende Prieto et al. (2001) in the case of oxygen, while solar abundances for the other elements were taken from Grevesse & Sauval (1998): Ne (photospheric), S (meteoritic), Cl (meteoritic), and Ar (photospheric). A representative error bar relevant to our data is given in each plot. Finally, we remind the reader that typically PN distances contain relatively large uncertainties, and thus some of the scatter in each of the figures is undoubtedly the result of this fact.

Table 7 gives the parameters and information related to linear fits to our results for the five elements in Figs. 6a-e. For each element indicated in the first column we give the y-intercept and slope, along with a correlation coefficient, number of sample objects included in the fitting, and the logarithmic offset from the solar value at the distance of 8.5 kpc, where the solar values are taken from the references cited in the previous paragraph.

Of particular interest are the slopes in column 3, since comparing values for Ne, S, Cl, and Ar with O may either confirm or argue against the often-assumed lockstep chemical evolution of the first four elements with the last one. We see that considering the uncertainties, all of the slopes agree with one another, and so we find no evidence in our data that such lockstep behavior does not take place. This is in qualitative agreement with Garnett’s (1989) conclusion following his detailed study of S in extragalactic H II regions.

For oxygen, Fig. 6a shows the consistency which exists among data from both nebular and stellar sources located in the disk. Our gradient of $-0.037\pm.008$ dex kpc^{-1} agrees within the uncertainties with the value derived by Deharveng et al., i.e. $-0.0395\pm.0049$ dex kpc^{-1} ; like them we see no suggestion that the gradient flattens in the outer regions. Our measurement is somewhat less than values given by Afflerbach et al., $-0.064\pm.009$ dex kpc^{-1} , Gummersbach et al., $-0.07\pm.02$ dex kpc^{-1} , and Rolleston et al., $-0.067\pm.008$ dex kpc^{-1} . Deharveng et al. obtain a correlation coefficient of -0.86, which is significantly better than our value of -0.45. It is very likely that the larger uncertainties inherent in PN distances explain much of this difference. We note, for example, that the coefficients reported by Maciel & Quireza (1999) for gradients derived from PNe are generally less than H II region values for the same element. Nevertheless, using our gradient, our interpo-

lated value for $12+\log(\text{O}/\text{H})$ at the solar circle (8.5 kpc) is 8.66, close to the solar measurement by Allende Prieto et al. (2001) of 8.69 as well as the one by Holweger (2001) of 8.74. We mention that while distances to B stars are likely to be much better known than PN distances, these objects nevertheless exhibit some scatter in Fig. 6a, suggesting that PN distances are not likely to be the only important source of scatter.

It is interesting to note that inside the solar circle our data are compatible with a relatively flat abundance gradient, with a slight steepening beyond that point. We point out that we do not see evidence for a flatter gradient in the outer disk compared with the inner regions, as reported by Vílchez and Esteban (1996) and Maciel & Quireza (1999), although our observations may be consistent with the report by Twarog, Ashman, and Anthony-Twarog (1996) of a discontinuity in $[\text{Fe}/\text{H}]$ along the Milky Way disk, where $[\text{Fe}/\text{H}]$ dropped by 0.3 dex beyond 10 kpc. However, we observed only a few PNe beyond 10 kpc.

Turning to Ne in Fig. 6b, we see that our data are consistent with measurements by Shaver et al. (1983). Our gradient of $-0.044\pm.014$ agrees within the uncertainties with Maciel & Quireza’s measurement of $-0.036\pm.010$. Our interpolated Ne abundance at the Sun’s location is 8.00, close to the Grevesse & Sauval (1998) number of 8.08. Additional comparison values for the solar vicinity are 7.89 for Orion (Esteban et al. 1998) and 8.13 for M17 (Peimbert, Torres-Peimbert, & Ruiz 1992). However, there is suprisingly little Ne abundance data available especially for H II regions inside the solar circle; it would be very interesting to probe the Ne gradient in the Milky Way disk to a greater extent than has been done in the past.

The sulfur data displayed in Fig. 6c show the sulfur anomaly (see §4.2) clearly, as our PN data are shifted downward systematically by about 0.5 dex from H II regions. We see also the relatively larger amount of scatter in the PN abundances than in the H II regions. Our S gradient of $-0.048\pm.0098$ dex kpc^{-1} is flatter than Maciel & Quireza’s value of $-0.077\pm.011$ dex kpc^{-1} , while our interpolated solar S abundance is 6.64 compared with the meteoritic measurement of 7.20 in Grevesse & Sauval. However, in light of the discussion of the S anomaly above, it is questionable whether PNe can currently be used to probe the galactic S gradient. Finally, the Cepheid abundances are systematically greater than those for H II regions by about 0.5 dex.

Fig. 6d shows our results for Cl, where PN data from Maciel & Chiappini (1994) are included only for comparison purposes, since many of the objects in the two samples are the same. Clearly there is significant scatter in both samples, which is perhaps explained by the relatively weak emission lines associated with Cl. We measure a gradient of $-0.045\pm.013$ dex kpc^{-1} , compared with Maciel & Chiappini’s steeper value of $-0.07\pm.01$ dex kpc^{-1} . Our interpolated solar value is 5.07, slightly smaller than Grevesse & Sauval’s measurement of 5.28 in the Sun. While Cl abundances in H II regions over a large range of galactocentric distances are in short supply [Rodríguez (1999) reports ionic abundances but no separate elemental abundances for the seven Galactic H II regions studied], Esteban et al. (1998) find a value of 5.33 in Orion, while Peimbert et al. (1992) infer a level of 5.48 in M17, both somewhat larger than our value for the solar vicinity.

Finally, our Ar measurements are displayed in Fig. 6e. The PN and H II region data sets are very consistent but with some scatter. We find a gradient of -0.030 ± 0.010 dex kpc^{-1} , while Maciel & Quireza measure a steeper gradient of -0.051 ± 0.010 dex kpc^{-1} . Our interpolated solar Ar value is 6.33, while Grevesse & Sauval’s photospheric number is 6.40, close to ours. Additional comparisons are 6.49 for Orion (Esteban et al.) and 6.63 for M17 (Peimbert et al.).

In summary, each of the five elements, O, Ne, S, Cl, and Ar shows a negative gradient with galactocentric distance, as anticipated. The consistency of the slopes among the five elements that we studied adds support to the idea that these elements increase globally in lockstep. The most interesting result continues to be the systematic offset in sulfur abundances between H II regions and PNe (Fig. 6c).

6. CONCLUSIONS

This paper is the culmination of a project whose object is to study the abundances of S, Cl, and Ar in planetary nebulae in detail. We carefully selected a sample of 86 PNe spanning a large range in galactocentric distance but representing primarily the Galactic disk population. A few halo PNe, however, were included in our sample.

We observed each object spectroscopically between 3600-9600 Å with the express purpose of including the strong nebular NIR lines of [S III] in our data for each object. Additionally, we have used our data to compute ionic and elemental abundances for these three elements. Our purpose has been to produce a large, homogeneous set of chemical abundances.

In considering the resulting electron temperatures derived from our data for each object, we found only weak correlations between most of them with the exception of the [O III] and [S III] temperatures. For this last case, we discuss a close direct relation between these two temperatures, possibly related to the fact that they occupy similar regions of the nebula and that both are associated with lines with high critical density, well above those encountered in PNe.

In compiling our abundance results we found a strong correlation between Ne and O, the robust relation that is consistent with earlier work by ourselves and others. Likewise, Cl and Ar abundances are correlated with O but with much more scatter in the relation. Our average abundance ratios of Cl/O, and Ar/O proved to be very consistent with those derived in other PN studies as well as studies of H II regions and the Sun. We also found that our average S/O ratio was somewhat below previous findings by other researchers, but still within the scatter and uncertainty of most determinations.

The most interesting correlation is the one between S and O. When compared with similar data for stars and H II regions, we find that many PNe have much lower S abundances than expected given their O abundances, a result we have called the S anomaly. We emphasize that this is not a new result, as it appears in others’ data as well when the same comparisons are made. Our result

merely represents the first time that it has been *noticed* on such a large scale. We also point out that H II regions appear not to suffer from this anomaly. In an attempt to discover the anomaly's cause, we have looked carefully at our abundance method for S, comparing with others' results as well as our own detailed photoionization models. We have also employed our ionization correction factor to estimate the amount of unseen S and compared our implied amounts directly with observed ones for the few cases where both types of data are available.

While we were unable to establish with certainty the cause of the S anomaly, we feel it is most likely due to excess amounts of S^{+3} in many nebulae beyond what is implied by models or inferred directly from observations of S^+ and S^{+2} . Thus, this additional S escapes indirect detection when an ICF is used. Our conclusion is supported by our finding that most direct determinations of S^{+3} using IR spectroscopy imply a larger amount of this ion than is inferred indirectly when only optical spectra are used. This result is uncertain, however, because of inconsistencies in aperture size and nebular position between the observations of the two different spectral regions. In addition, by calculating the amount of S^{+3} necessary to explain the S deficit for each object, we find that there is an inverse correlation between this amount and the O^{+2}/O abundance ratio, consistent with the idea that the deficit is greater in low excitation nebulae.

Finally, we analyzed our abundance data in terms of galactocentric distance. We found evidence for abundance gradients for O, Ne, S, Cl, and Ar; due to scatter in the others, the relation for O is the most definite and convincing. Our computed slopes were found to be somewhat smaller but nevertheless compatible with other published results.

We thank the TACs at KPNO & CTIO for granting us observing time, the local staff there for their assistance, and the IRAF staff for their ready answers. We appreciate the contributions of Jackie Milingo to the data reductions and abundance analysis for a large fraction of the sample early-on. We are extremely grateful to M.J. Barlow and X.-W. Liu and to D. Beintema and J. Bernard-Salas for providing the ISO SWS line fluxes, to Walter Maciel for sending us his PN chlorine data in electronic form, to Georges Meynet for responding to our numerous questions regarding nucleosynthesis, to Don Garnett for reading and offering suggestions for improvement on an earlier version of the manuscript, and to an anonymous referee for making numerous suggestions for improving the paper. We also thank the following students for their assistance with various calculations related to this project: Lissa Ong (Williams '04) and Davis Stevenson (Williams '04), both supported by a grant from the Bronfman Science Center at Williams College; and Megan Roscioli (Haverford '05) a Keck Summer Fellow at Williams College supported by the Keck Northeast Astronomy Consortium. KBK also acknowledges support from the Bronfman Science Center and the Dean of the Faculty at Williams College. Finally, we thank the NSF for support for this entire project under grant AST-9819123 to Williams College and AST-0307118 to the University of Oklahoma.

APPENDIX A

Ten objects whose line strengths were measured and reported as part of an earlier series of papers were added to the current sample because abundances of S, Cl, and Ar were not previously computed. Table 8a gives the resulting ion abundances, ICFs, electron temperatures and densities for these objects. Line strength sources are provided in the table footnotes. The elemental abundances for these objects are provided in Table 8b. Note that electron temperatures deemed very unreliable have been set off with parentheses in Table 8a.

APPENDIX B

The values S^{+3}/H^{+} in column 3 of Table 6 which are given for IC3568, IC4593, NGC 6210, NGC 6572, NGC 6884, and NGC 7027 were calculated from line strength data provided in Table 1 of Dinerstein (1980b). We first used our own values for $H\alpha$ and $[N II]$ line strengths to derive $H\alpha$ from Dinerstein's $H\alpha+[N II]$ value. We then multiplied the ratio of her $[S IV] 10.5\mu m:H\alpha$ by our observed $H\alpha/H\beta$ ratio to give the $[S IV]/H\beta$ ratio uncorrected for reddening. This ratio was then multiplied by 10^{cf} to correct for reddening, where we took $f=-1.09$ and c was taken from our own observations. This dereddened $[S IV]/H\beta$ ratio was then used in a 5-level atom calculation along with our observed $[O III]$ temperatures and $[S II]$ densities to finally derive the S^{+3}/H^{+} ratio. Collision strengths were taken from Tayal (2000).

Table 1. Abundance Compilation

Object	Type	He/H	O/H($\times 10^4$)	Ne/O	S/O($\times 10^1$)	Cl/O($\times 10^3$)	Ar/O($\times 10^2$)	N/O	Dist.(kpc) ^a	Ref ^b
BB1	halo	0.09 (± 0.03)	0.78 (± 1.1)	1.63 (± 0.23)	0.01 (± 0.01)	...	0.02 (± 0.01)	0.64 (± 0.11)	16.5	3
Cn 2-1	II	0.13 (± 0.04)	7.14 (± 1.0)	0.23 (± 0.03)	0.09 (± 0.01)	0.25 (± 0.04)	0.38 (± 0.05)	0.39 (± 0.06)	2.4	2
DdDm 1	halo	0.10 (± 0.03)	1.38 (± 0.20)	0.17 (± 0.02)	0.18 (± 0.06)	0.15 (± 0.05)	0.37 (± 0.12)	0.21 (± 0.03)	11.4	4
Fg 1	II	0.13 (± 0.04)	3.73 (± 0.53)	0.29 (± 0.04)	0.12 (± 0.02)	0.33 (± 0.10)	0.57 (± 0.08)	0.43 (± 0.06)	8.0	2
H 4-1	halo	0.12 (± 0.04)	1.99 (± 0.28)	0.02 (± 0.01)	0.01 (± 0.001)	...	0.01 (± 0.001)	0.29 (± 0.04)	15.1	3
Hb 12	II	0.08 (± 0.02)	0.37 (± 0.05)	0.27 (± 0.04)	0.55 (± 0.17)	0.18 (± 0.11)	1.78 (± 1.1)	0.45 (± 0.08)	13.8	3
He 2-21	II	0.12 (± 0.04)	2.99 (± 0.42)	0.16 (± 0.02)	0.06 ^c (± 0.01)	0.28 (± 0.04)	0.36 (± 0.05)	0.15 (± 0.02)	11.5	2
He 2-37	II	0.12 (± 0.04)	11.0 (± 1.6)	0.23 (± 0.03)	0.04 (± 0.01)	0.27 (± 0.04)	0.43 (± 0.06)	0.32 (± 0.05)	9.2	2
He 2-48	II	0.11 (± 0.03)	4.23 (± 0.60)	0.27 (± 0.04)	0.05 ^c (± 0.02)	0.19 (± 0.12)	0.25 (± 0.15)	0.31 (± 0.04)	8.9	2
He 2-55	II	0.13 (± 0.04)	6.87 (± 0.97)	0.26 (± 0.04)	0.08 ^c (± 0.01)	0.53 (± 0.32)	0.73 (± 0.10)	0.20 (± 0.03)	8.2	2
He 2-115	II	0.12 (± 0.04)	3.50 (± 0.49)	0.13 (± 0.02)	0.08 (± 0.03)	0.26 (± 0.08)	0.63 (± 0.09)	0.17 (± 0.03)	6.2	2
He 2-123	I	0.15 (± 0.05)	6.52 (± 0.92)	0.27 (± 0.04)	0.16 ^c (± 0.02)	0.50 (± 0.16)	0.61 (± 0.09)	0.81 (± 0.11)	6.0	2
He 2-138	II	...	4.60 (± 1.5)	...	0.22 ^c (± 0.07)	0.35 (± 0.14)	6.2	2
He 2-140	II	0.08 (± 0.02)	3.82 (± 0.54)	0.09 (± 0.05)	0.34 (± 0.05)	0.46 (± 0.28)	0.58 (± 0.08)	0.38 (± 0.06)	5.3	2
He 2-141	II	0.12 (± 0.04)	7.64 (± 1.1)	0.19 (± 0.03)	0.04 ^c (± 0.01)	0.34 (± 0.05)	0.33 (± 0.04)	0.34 (± 0.05)	6.0	2
He 2-157	II	0.12 (± 0.04)	1.69 (± 0.24)	...	0.38 ^c (± 0.05)	0.39 (± 0.06)	0.68 (± 0.10)	0.40 (± 0.06)	3.5	2
He 2-158	II	0.12 (± 0.04)	3.24 (± 0.46)	0.22 (± 0.03)	0.13 (± 0.02)	0.25 (± 0.15)	0.46 (± 0.07)	0.31 (± 0.04)	11.1	2
Hu 2-1	II	0.10 (± 0.03)	2.43 (± 0.34)	0.13 (± 0.02)	0.06 (± 0.01)	0.17 (± 0.05)	0.55 (± 0.08)	0.26 (± 0.05)	7.2	3
IC418	II	0.07 (± 0.02)	1.39 (± 0.20)	0.05 (± 0.01)	0.53 (± 0.17)	...	0.80 (± 0.25)	0.59 (± 0.08)	9.3	4
IC1297	II	0.13 (± 0.04)	7.20 (± 1.0)	0.24 (± 0.03)	0.10 (± 0.01)	0.27 (± 0.04)	0.37 (± 0.05)	0.31 (± 0.04)	5.2	2
IC2165	II	0.09 (± 0.03)	3.11 (± 0.44)	0.22 (± 0.03)	0.09 (± 0.01)	0.22 (± 0.03)	0.51 (± 0.07)	0.43 (± 0.06)	10.5	3
IC2448	II	0.12 (± 0.04)	3.25 (± 2.0)	0.21 (± 0.13)	0.21 ^c (± 0.13)	0.21 (± 0.13)	0.38 (± 0.23)	0.29 (± 0.18)	8.3	2
IC2501	II	...	4.25 (± 0.60)	0.26 (± 0.04)	0.06 (± 0.01)	0.22 (± 0.03)	0.41 (± 0.06)	0.34 (± 0.05)	8.4	2
IC2621	I	0.12 (± 0.04)	4.55 (± 0.64)	0.23 (± 0.03)	0.14 (± 0.02)	0.33 (± 0.05)	0.87 (± 0.12)	0.84 (± 0.15)	7.9	2
IC3568	II	0.12 (± 0.04)	3.77 (± 0.53)	0.19 (± 0.03)	0.03 (± 0.01)	0.09 (± 0.03)	0.28 (± 0.09)	0.05 (± 0.01)	10.2	4
IC4593	II	0.10 (± 0.03)	4.98 (± 0.70)	0.18 (± 0.03)	0.08 (± 0.03)	0.18 (± 0.06)	0.37 (± 0.05)	0.06 (± 0.01)	6.9	4
IC4776	II	0.11 (± 0.03)	4.58 (± 0.65)	0.22 (± 0.03)	0.14 (± 0.02)	0.23 (± 0.03)	0.36 (± 0.22)	0.33 (± 0.05)	5.0	2
IC5217	II	0.11 (± 0.03)	3.72 (± 0.53)	0.23 (± 0.03)	0.14 (± 0.02)	0.36 (± 0.11)	0.45 (± 0.06)	0.32 (± 0.06)	9.4	1
J320	II	0.11 (± 0.03)	2.49 (± 0.35)	0.21 (± 0.03)	0.08 ^c (± 0.01)	0.29 (± 0.04)	0.38 (± 0.05)	0.52 (± 0.07)	13.9	2
J900	II	0.10 (± 0.03)	3.54 (± 0.50)	0.25 (± 0.04)	0.06 (± 0.02)	0.11 (± 0.02)	0.34 (± 0.05)	0.29 (± 0.04)	11.8	3
K648	halo	0.10 (± 0.03)	0.71 (± 0.10)	0.14 (± 0.02)	0.03 (± 0.02)	...	0.06 (± 0.01)	0.04 (± 0.01)	10.2	3
M 1-5	II	0.11 (± 0.03)	1.29 (± 0.18)	0.09 (± 0.01)	0.20 (± 0.03)	0.38 (± 0.12)	0.77 (± 0.24)	0.45 (± 0.08)	13.5	2
M 1-25	II	0.15 (± 0.05)	5.03 (± 0.71)	0.07 (± 0.01)	0.18 (± 0.03)	0.40 (± 0.06)	0.66 (± 0.09)	0.44 (± 0.06)	3.7	2
M 1-34	I	0.15 (± 0.05)	6.79 (± 0.96)	0.40 (± 0.06)	0.19 (± 0.03)	0.33 (± 0.05)	0.43 (± 0.14)	0.66 (± 0.14)	2.6	2
M 1-38	II	...	5.91 (± 0.55)	...	0.12 ^c (± 0.04)	...	0.03 (± 0.02)	0.21 (± 0.07)	2.0	2
M 1-50	II	0.12 (± 0.04)	6.40 (± 0.91)	0.21 (± 0.03)	0.07 (± 0.01)	0.30 (± 0.18)	0.38 (± 0.05)	0.18 (± 0.03)	4.3	1,2 ^d
M 1-54	I	0.15 (± 0.05)	5.71 (± 0.81)	0.39 (± 0.06)	0.21 (± 0.03)	0.35 (± 0.11)	0.45 (± 0.06)	1.06 (± 0.15)	4.8	1,2 ^d
M 1-57	I	0.13 (± 0.04)	6.42 (± 0.91)	0.21 (± 0.03)	0.16 ^c (± 0.02)	0.42 (± 0.13)	0.74 (± 0.10)	1.02 (± 0.14)	5.3	1
M 1-74	I	0.12 (± 0.04)	4.74 (± 0.67)	0.25 (± 0.04)	0.30 (± 0.04)	0.22 (± 0.13)	0.69 (± 0.10)	0.91 (± 0.13)	7.5	1
M 1-80	II	0.10 (± 0.03)	8.79 (± 1.2)	0.21 (± 0.03)	0.05 (± 0.01)	0.06 (± 0.04)	0.29 (± 0.04)	0.39 (± 0.06)	11.3	1
M 2-10	II	0.13 (± 0.04)	6.05 (± 0.86)	0.25 (± 0.04)	0.18 ^c (± 0.03)	0.45 (± 0.27)	0.57 (± 0.08)	0.50 (± 0.07)	2.5	2
M 3-4	II	0.15 (± 0.05)	5.16 (± 0.73)	0.34 (± 0.05)	0.03 (± 0.01)	0.16 (± 0.05)	0.28 (± 0.04)	0.37 (± 0.05)	17.1	2
M 3-6	II	0.12 (± 0.04)	5.59 (± 0.79)	0.24 (± 0.03)	0.13 (± 0.02)	0.21 (± 0.13)	0.55 (± 0.08)	0.10 (± 0.01)	9.9	2
M 3-15	II	0.13 (± 0.04)	7.60 (± 1.1)	0.20 (± 0.03)	0.11 ^c (± 0.02)	0.33 (± 0.20)	0.42 (± 0.06)	0.36 (± 0.05)	7.0	1,2 ^d
NGC 650	II	0.11 (± 0.03)	7.11 (± 1.0)	0.39 (± 0.06)	0.13 (± 0.02)	0.06 (± 0.02)	0.52 (± 0.07)	0.54 (± 0.08)	9.6	3
NGC 1535	II	0.08 (± 0.02)	2.66 (± 0.38)	0.27 (± 0.04)	0.25 (± 0.08)	0.16 (± 0.02)	0.36 (± 0.05)	0.20 (± 0.03)	10.1	3

Table 1—Continued

Object	Type	He/H	O/H($\times 10^4$)	Ne/O	S/O($\times 10^1$)	Cl/O($\times 10^3$)	Ar/O($\times 10^2$)	N/O	Dist.(kpc) ^a	Ref ^b
NGC 2022	II	0.09 (± 0.03)	7.50 (± 1.1)	0.19 (± 0.03)	0.10 (± 0.03)	0.61 (± 0.19)	1.24 (± 0.18)	0.12 (± 0.02)	11.0	3
NGC 2371	II	0.10 (± 0.03)	7.71 (± 1.1)	0.23 (± 0.03)	0.10 (± 0.03)	0.61 (± 0.09)	1.32 (± 0.19)	0.39 (± 0.06)	10.5	3
NGC 2392	II	0.08 (± 0.02)	3.75 (± 0.53)	0.28 (± 0.04)	0.15 (± 0.09)	...	0.43 (± 0.14)	0.30 (± 0.04)	9.8	4
NGC 2438	II	0.09 (± 0.03)	5.24 (± 0.74)	0.32 (± 0.05)	0.13 (± 0.04)	...	0.42 (± 0.06)	0.43 (± 0.06)	9.9	3
NGC 2440	I	0.10 (± 0.03)	5.19 (± 0.73)	0.21 (± 0.03)	0.05 (± 0.01)	0.53 (± 0.17)	0.78 (± 0.11)	2.05 (± 0.29)	9.5	3
NGC 2792	II	0.11 (± 0.03)	7.65 (± 2.4)	0.16 (± 0.05)	0.07 ^c (± 0.02)	0.68 (± 0.22)	0.84 (± 0.27)	0.18 (± 0.11)	8.8	2
NGC 2867	II	0.12 (± 0.04)	5.23 (± 0.74)	0.21 (± 0.03)	0.06 (± 0.01)	0.28 (± 0.04)	0.37 (± 0.05)	0.26 (± 0.04)	8.4	2
NGC 3195	II	0.13 (± 0.04)	6.88 (± 0.97)	0.40 (± 0.06)	0.15 (± 0.02)	0.23 (± 0.14)	0.40 (± 0.06)	0.45 (± 0.06)	7.7	2
NGC 3211	II	0.11 (± 0.03)	8.38 (± 1.2)	0.16 (± 0.02)	0.07 ^c (± 0.01)	0.54 (± 0.08)	0.76 (± 0.11)	0.20 (± 0.03)	8.2	2
NGC 3242	II	0.11 (± 0.03)	4.10 (± 0.58)	0.21 (± 0.03)	0.05 (± 0.01)	0.26 (± 0.04)	0.36 (± 0.05)	0.12 (± 0.04)	8.7	2 ^e
NGC 3587	II	0.10 (± 0.03)	4.53 (± 0.64)	0.27 (± 0.04)	0.08 (± 0.01)	...	0.24 (± 0.15)	0.21 (± 0.03)	9.3	1
NGC 3918	II	0.11 (± 0.03)	5.54 (± 0.78)	0.19 (± 0.03)	0.05 (± 0.01)	0.36 (± 0.05)	0.61 (± 0.09)	0.39 (± 0.06)	8.1	3
NGC 5307	II	0.10 (± 0.03)	3.85 (± 0.54)	0.23 (± 0.03)	0.05 (± 0.03)	0.18 (± 0.06)	0.35 (± 0.05)	0.13 (± 0.02)	6.9	2
NGC 5882	II	0.12 (± 0.04)	5.48 (± 0.77)	0.27 (± 0.04)	0.13 (± 0.02)	0.31 (± 0.04)	0.51 (± 0.07)	0.33 (± 0.05)	7.1	3
NGC 6210	II	0.11 (± 0.03)	5.21 (± 0.74)	0.25 (± 0.04)	0.13 (± 0.04)	0.27 (± 0.04)	0.34 (± 0.05)	0.22 (± 0.03)	7.6	4
NGC 6309	II	0.13 (± 0.04)	6.58 (± 0.93)	0.22 (± 0.03)	0.08 (± 0.03)	0.60 (± 0.36)	0.82 (± 0.12)	0.28 (± 0.04)	6.3	1,2 ^d
NGC 6439	I	0.14 (± 0.04)	6.32 (± 0.89)	0.27 (± 0.04)	0.17 (± 0.02)	0.44 (± 0.14)	0.53 (± 0.07)	0.80 (± 0.11)	4.0	1,2 ^d
NGC 6563	II	0.12 (± 0.04)	6.37 (± 0.90)	0.33 (± 0.05)	0.06 ^c (± 0.01)	0.05 (± 0.03)	0.30 (± 0.04)	0.32 (± 0.05)	6.2	2
NGC 6565	II	0.12 (± 0.04)	7.25 (± 1.0)	0.33 (± 0.05)	0.13 (± 0.02)	0.26 (± 0.04)	0.33 (± 0.05)	0.41 (± 0.06)	4.2	2
NGC 6567	II	0.10 (± 0.03)	2.67 (± 0.38)	0.18 (± 0.03)	0.06 (± 0.01)	0.18 (± 0.06)	0.21 (± 0.03)	0.23 (± 0.04)	6.0	3
NGC 6572	I	0.13 (± 0.04)	4.29 (± 0.61)	0.23 (± 0.03)	0.10 (± 0.01)	0.23 (± 0.07)	0.53 (± 0.07)	0.67 (± 0.12)	7.7	1
NGC 6578	II	0.12 (± 0.04)	7.42 (± 1.0)	0.30 (± 0.04)	0.11 (± 0.02)	0.25 (± 0.08)	0.43 (± 0.06)	0.31 (± 0.04)	6.1	3
NGC 6629	II	0.11 (± 0.03)	4.50 (± 0.64)	0.20 (± 0.03)	0.07 (± 0.01)	0.21 (± 0.03)	0.42 (± 0.06)	0.14 (± 0.02)	6.7	2
NGC 6720	II	0.12 (± 0.04)	7.64 (± 1.1)	0.27 (± 0.04)	0.06 (± 0.02)	0.32 (± 0.05)	0.56 (± 0.08)	0.35 (± 0.05)	8.1	4
NGC 6790	II	0.12 (± 0.04)	3.36 (± 0.48)	0.17 (± 0.02)	0.06 (± 0.01)	0.18 (± 0.11)	0.26 (± 0.04)	0.18 (± 0.03)	6.3	1
NGC 6826	II	0.11 (± 0.03)	4.16 (± 0.59)	0.20 (± 0.03)	0.07 (± 0.02)	0.20 (± 0.03)	0.36 (± 0.11)	0.12 (± 0.02)	8.5	4
NGC 6879	II	0.11 (± 0.03)	3.79 (± 0.54)	0.22 (± 0.03)	0.09 (± 0.03)	0.15 (± 0.09)	0.39 (± 0.06)	0.18 (± 0.03)	7.5	1
NGC 6884	II	0.12 (± 0.04)	5.55 (± 0.78)	0.22 (± 0.03)	0.11 (± 0.02)	0.35 (± 0.11)	0.54 (± 0.08)	0.41 (± 0.07)	5.9	1
NGC 6886	II	0.12 (± 0.04)	5.24 (± 0.74)	0.23 (± 0.03)	0.11 (± 0.02)	0.42 (± 0.13)	0.78 (± 0.11)	0.43 (± 0.08)	7.5	1
NGC 6891	II	0.11 (± 0.03)	4.25 (± 0.60)	0.19 (± 0.03)	0.04 (± 0.01)	0.16 (± 0.05)	0.39 (± 0.24)	0.10 (± 0.02)	7.3	1
NGC 7009	II	0.12 (± 0.04)	5.63 (± 0.80)	0.23 (± 0.03)	0.15 (± 0.05)	0.32 (± 0.05)	0.47 (± 0.07)	0.42 (± 0.06)	7.8	4
NGC 7026	I	0.14 (± 0.04)	7.31 (± 1.0)	0.30 (± 0.04)	0.21 (± 0.03)	0.50 (± 0.16)	0.73 (± 0.10)	0.76 (± 0.11)	8.7	1
NGC 7027	II	0.10 (± 0.03)	4.15 (± 0.59)	0.17 (± 0.02)	0.13 (± 0.02)	0.41 (± 0.06)	0.65 (± 0.09)	0.56 (± 0.08)	8.5	3
NGC 7293	II	0.13 (± 0.04)	6.47 (± 0.91)	0.65 (± 0.09)	0.09 (± 0.03)	...	0.48 (± 0.07)	0.36 (± 0.05)	8.2	4
NGC 7662	II	0.10 (± 0.03)	4.19 (± 0.59)	0.17 (± 0.02)	0.10 (± 0.01)	0.50 (± 0.07)	0.59 (± 0.08)	0.18 (± 0.03)	8.9	3
PB 6	I	0.17 (± 0.05)	6.77 (± 0.96)	0.24 (± 0.03)	0.03 (± 0.004)	0.27 (± 0.04)	0.87 (± 0.12)	1.13 (± 0.16)	9.0	2
PC 14	II	0.12 (± 0.04)	7.88 (± 1.1)	0.27 (± 0.04)	0.09 (± 0.01)	0.26 (± 0.16)	0.38 (± 0.05)	0.18 (± 0.03)	4.4	2
Pe 1-18	I	0.14 (± 0.04)	4.56 (± 0.64)	0.21 (± 0.03)	0.21 (± 0.03)	0.40 (± 0.13)	0.72 (± 0.10)	1.70 (± 0.30)	3.9	1,2 ^d
Th 2-A	II	0.13 (± 0.04)	6.23 (± 0.88)	0.31 (± 0.04)	0.07 (± 0.02)	0.12 (± 0.02)	0.52 (± 0.32)	0.49 (± 0.07)	7.2	2
Averages ^f										
Type I	...	0.137 \pm 0.018 (12)	5.76 \pm 1.06 (12)	0.27 \pm 0.066 (12)	0.16 \pm 0.075 (12)	0.38 \pm 0.11 (12)	0.66 \pm 0.15 (12)	1.03 \pm 0.49 (12)
Type II	...	0.113 \pm 0.016 (66)	5.09 \pm 2.02 (69)	0.23 \pm 0.085 (66)	0.12 \pm 0.097 (69)	0.29 \pm 0.14 (62)	0.50 \pm 0.27 (68)	0.31 \pm 0.14 (69)
Halo	...	0.103 \pm 0.011 (4)	1.00 \pm 0.64 (5)	0.41 \pm 0.61 (5)	0.058 \pm 0.071 (4)	0.13 \pm 0.11 (2)	0.12 \pm 0.15 (4)	0.33 \pm 0.27 (4)
All	...	0.115 \pm 0.018 (82)	5.01 \pm 2.04 (86)	0.25 \pm 0.17 (83)	0.12 \pm 0.095 (85)	0.30 \pm 0.14 (76)	0.51 \pm 0.27 (84)	0.41 \pm 0.35 (85)

^aGalactocentric distances were calculated from heliocentric distances given by Maciel (1984) for H4-1, He2-48, He2-55, and M3-15; Cahn et al (1992) for DdDm-1 and Hu2-1; Sabbadin (1986) for K648; Torres-Peimbert et al. (1990) for BB1; and Zhang (1995) for the rest. A solar galactocentric distance of 8.5 kpc was assumed.

^bAbundance references: 1=Kwitter & Henry (2001); 2=Milingo, Henry, & Kwitter (2002); 3=Kwitter, Henry, & Milingo (2003); 4=Appendix A, this paper.

^cS/O value differs slightly from the one(s) originally published in the earlier reference(s) due to an improvement in the estimated electron temperature relevant for this object. This value supersedes the former one.

^dValues quoted are averages of abundances from the two sources

^eValues quoted are averages of positions A and B abundances

^fThe values in parentheses indicate the number of sample objects included in the average.

Table 2. Electron Temperatures and Densities^a

Object	T _[O III] (K)	T _[N II] (K)	T _[O II] (K)	T _[S II] (K)	T _[S III] (K)	N _e (cm ⁻³)
BB1	12400	10500	8000	7100 ^c
Cn 2-1	9600	10200	13700	13300	12000	4100
DdDm1	11700	11400	10100	7900	12700	4000
Fg 1	9300	8300	7100	...	9400	600
H4-1	12300	10200	6100	400
Hb 12	18500	9300	6300
He 2-21	12200	7600	11500	...	17600	1500
He 2-37	12000	10000	14500	10300	13800	200
He 2-48	11200	9600	...	6500	...	10
He 2-55	12200	9500	16100	...	17200	200
He 2-115	9100	10100	12400	16300	11500	11700
He 2-123	6200	6600	5800	6400	7700	2000
He 2-138	5800	5600	5900	6300	...	5300
He 2-140	7000	7100	7100	6100	8200	5300
He 2-141	12400	8800	7300	...	15500	1400
He 2-157	10500	9900	7400	...	9800	5200
He 2-158	9200	10000	7800	15200	9700	2400
Hu 2-1	9100	11700	20600	...	11100	8500
IC418	8500	10700	17100	8700	8100	3300
IC1297	9900	8900	8100	...	11000	2400
IC2165	13000	12700	9800	10300	14200	4100
IC2448	12500	10
IC2501	9500	11200	10600	11700	12700	4800
IC2621	12500	11200	12800	8300
IC3568	10400	6700	8800	...	10300	800
IC4593	8100	7300	6800	...	9000	1700
IC4776	9500	13500	15600	15000	11500	4000
IC5217	11000	10700	12300	8800	11200	10000
J320	12100	9900	16100	6100	17600	4600
J900	11600	11500	10300	7800 ^b	13000	3600
K648	11800	9200	8400	1000
M1-5	10000	10100	...	11700	10100	6400
M1-25	8400	8200	7900	9100	9300	4300
M1-34	9200	8200	5400	9400	9100	700
M1-38	6300	6300	5900	6600	8500	5100
M1-50	10300	10400	11700	...	12900	4500
M1-54	9800	8700	6200	11200	9200	1500
M1-57	12300	11200	13000	6700	15800	4500
M1-74	9300	14700	11400	2100
M1-80	9500	10000	6200	10400	13500	800
M2-10	6300	6700	5100	11400	7200	1300
M3-4	11500	9300	14000	8500	11000	200
M3-6	8000	8700	9500	...	8400	1700
M3-15	8000	10400	10800	9000	10500	3700
NGC 650	10800	9700	14800	10300	13300 ^b	200
NGC 1535	11400	...	7400	...	17900 ^c	300

Table 2—Continued

Object	$T_{[\text{O III}]} \text{ (K)}$	$T_{[\text{N II}]} \text{ (K)}$	$T_{[\text{O II}]} \text{ (K)}$	$T_{[\text{S II}]} \text{ (K)}$	$T_{[\text{S III}]} \text{ (K)}$	$N_e \text{ (cm}^{-3}\text{)}$
NGC 2022	13600	10300	7500	...	19600	800
NGC 2371	12100	8600 ^b	6800	11400 ^c	13300	1000
NGC 2392	11900	11400	6800	...	10400	2000
NGC 2438	10300	10400 ^b	13100	9700 ^c	10000 ^c	200
NGC 2440	12600	10300	8300	13800 ^c	13800 ^b	1800
NGC 2792	13700	10200	7900	2800
NGC 2867	11200	10100	8200	...	12800	2100
NGC 3195	8900	8000	11300	12500	9000	200
NGC 3211	13300	10300	6700	1200
NGC 3242	11200	12100	9600	...	15800	2100
NGC 3587	10600	9400	11600	...	12400	100
NGC 3918	12200	10400	8500	8600	15300	3800
NGC 5307	12300	11000	9900	2600
NGC 5882	9100	9900	9900	...	10100	2200 ^b
NGC 6210	9400	10200	10100	9200	9500	4100
NGC-6309	11600	8900	10100	12000	11400	3600
NGC 6439	9700	9500	9000	6700	10000	4100
NGC 6563	10300	9000	13100	100
NGC 6565	10100	9400	6100	11800	10300	1300
NGC 6567	11000	12600 ^b	11800	16300 ^c	14500	6700 ^c
NGC 6572	10100	12300	11500	9500
NGC 6578	7800	10000	9000	...	9300	2400 ^b
NGC 6629	8500	10300	6500	...	9200	1100
NGC 6720	11050	9400	5800	12900	11400	600
NGC 6790	12400	18300	14800	>10000
NGC 6826	8900	8700	6700	...	9900	1700
NGC 6879	10100	8900	12700	15800	10400	7400
NGC 6884	10400	9900	11600	14400	10500	6500
NGC 6886	12100	9800	10300	8200	12900	7200
NGC 6891	9200	10600	9200	...	11500	10000
NGC 7009	9500	10200	10600	13900	10600	4300
NGC 7026	8500	9400	7800	6400	9500	3300
NGC 7027	13600	20100	15100	81000
NGC 7293	9100	8500	8600	13600	5100	100
NGC 7662	12700	10300	12200	...	13600	2700
PB 6	14600	9800	7600	...	16300	2200
PC 14	8800	8200	7400	6900	10200	2200
Pe 1-18	9800	12600	12500	12100
Th 2-A	11600	11700	5900	1200

^aTemperature and density uncertainties are each $\pm 10\%$, unless otherwise noted.

^bUncertainty estimated to be $\pm 20\%$

^cUncertainty estimated to be $\pm 30\%$

Table 3. Comparison of Abundance Ratio Averages

Paper ^a	log(S/O)	log(Cl/O)	log(Ar/O)	Comments
Planetary Nebulae ^b				
GM88	-1.87 (11)	...	-1.94 (3)	Galactic
FP91	-1.84 (8)	...	-2.25 (8)	Type I galactic
FP92	-1.95 (12)	...	-1.95 (17)	Type II galactic
FP93a	-1.63 (15)	...	-2.47 (15)	non-Type I in LMC
FP93b	-1.57 (8)	...	-2.16 (8)	Type I in LMC
KB94	-1.77 (43)	...	-2.32 (42)	Galactic
T03	-1.70 (15)	-3.44 (14)	-2.29 (14)	Galactic
This Paper	-1.91 (85)	-3.52 (75)	-2.29 (84)	Galactic
H II Regions ^b				
R99	-1.45	-3.30	-2.05	Ave., 7 Galactic
E98	-1.46	-3.30	-1.83	Orion Nebula
P92	-1.49	-3.33	-2.18	M17
KBG	-1.55 (19)	...	-2.21 (16)	20 H II Regions in M101 (Ave)
L02	-1.46	-3.54	-2.35	N5461 in M101
L02	-1.57	-3.67	-2.38	N5471 in M101
Sun				
GS98	-1.49	-3.41	-2.29	

^aGM88=Gutiérrez-Moreno & Moreno (1988); FP91=Freitas Pacheco, Maciel, Costa, & Barbuy (1991); FP92=Freitas Pacheco, Maciel, & Costa (1992); FP93a=Freitas Pacheco, Costa, & Maciel (1993a); FP93b=Freitas Pacheco, Barbuy, Costa, & Idiart (1993b); KB94=Kingsburgh & Barlow (1994); T03=Tsamis et al. (2003); R99=Rodríguez (1999); E98=Esteban et al. (1998; gas phase abundance values from their Table 17); P92=Peimbert et al. (1992); KBG=Kennicutt, Bresolin, & Garnett (2003); L02=Luridiana et al. (2002); GS98=Grevesse & Sauval (1998, where meteoritic values are used for S and Cl, photospheric value for Ar, but using the oxygen

abundance from Allende Prieto et al. 2001).

^bValues in parentheses indicate number of survey objects included in the computed average.

Table 4. $12+\log(X/H)$ vs. $12+\log(O/H)$: Fit Parameters

Quantity	Intercept	Slope	Corr. Coef.	Number
$12+\log(\text{Ne}/H)$	$-2.18\pm.83$	$1.18\pm.095$	0.81	82
$12+\log(\text{S}/H)$	-1.39 ± 1.17	$0.93\pm.14$	0.60	85
$12+\log(\text{Cl}/H)$	-5.27 ± 1.04	$1.20\pm.12$	0.76	75
$12+\log(\text{Ar}/H)$	-5.33 ± 1.20	$1.34\pm.14$	0.73	84

Table 5. Photoionization Models

Line ID/Parameter	IC 4593		Hu2-1		NGC 3242	
	Obs. ^a	Model	Obs. ^b	Model	Obs. ^c	Model
C IV λ 1549	5.8	1.4	...	1.8	36	115
C III] λ 1909	2.5	2.8	44	41	235	244
[O II] λ 3727	42	49	77	78	9.5	13
[Ne III] λ 3869	29	28	18	16	102	110
[S II] λ 4072	0.49	0.28	1.4	0.59	1.1:	0.11
C II λ 4267	0.17:	0.04	0.4:	0.14	0.75	0.25
[O III] λ 4363	1.9	1.9	2.3	2.6	13	14
He I λ 4471	4.9	5.4	4.9	4.9	3.9	4.2
He II λ 4686	0.67	0.32	0.2::	0.10	24	27
H β λ 4861	100	100	100	100	100	100
[O III] λ 5007	556	587	438	434	1275	1432
[Cl III] λ 5517	0.39	0.38	0.1::	0.16	0.30	0.44
[Cl III] λ 5537	0.35	0.37	0.3:	0.26	0.30	0.41
[N II] λ 5755	0.09::	0.11	2.3	1.2	0.10	0.04
He I λ 5876	15	16	15	15	12	13
[O I] λ 6300	...	0.01	2.3	0.03	...	<0.01
[S III] λ 6312	0.73	0.58	0.6	0.52	0.85	0.54
H α λ 6563	287	288	286	285	278	283
[N II] λ 6584	11	12	63	64	2.7:	2.3
[S II] λ 6716	0.55	0.90	0.4	0.46	0.35	0.27
[S II] λ 6731	0.78	1.3	0.9	0.92	0.45	0.37
[Ar III] λ 7135	9.7	11	10	14	8.7	9.3
[O II] λ 7325	2.4	1.7	29	11	1.2	0.73
[Ar III] λ 7751	2.3	2.6	2.4	3.3	2.0	2.2
[Cl IV] λ 8045	...	0.50	...	0.30	0.90	0.50
[S III] λ 9069	16:	16	5.2	10	6.0	7.8
[S III] λ 9532	45:	41	22	24	18	19
Model Parameters ^d						
He/H	0.10	0.11	0.11	0.10	0.11	0.11
C/H	3.98E-5	3.58E-5	4.35E-4	1.51E-4	3.28E-4	4.42E-4
N/H	2.99E-5	5.42E-5	6.32E-5	8.71E-5	4.92E-5	4.90E-5
O/H	4.98E-4	4.51E-4	2.43E-4	2.45E-4	4.10E-4	4.07E-4
Ne/H	8.96E-5	6.67E-5	3.16E-5	3.16E-5	8.61E-5	6.92E-5
S/H	3.98E-6	3.58E-6	1.46E-6	1.45E-6	2.05E-6	2.29E-6
Cl/H	8.96E-8	1.08E-7	4.13E-8	4.17E-8	1.07E-7	1.07E-7
Ar/H	1.84E-6	1.64E-6	1.34E-6	1.35E-6	1.48E-6	1.51E-6
T _{eff} (K)	40,000 ^e	48,000	38,000 ^f	41,000	75,000 ^e	90,000
log L _{Hβ} (erg/s)	34.5 ^g	34.8	34.1 ^g	34.2	34.4	34.8
N _e (cm ⁻³)	1700	1900	8500	8700	1700	1800
radius (pc)	0.098 ^g	0.13	0.018 ^g	0.036	0.098 ^g	0.12
filling factor	...	0.5	...	1	...	1

^aOptical and UV line strengths are taken from Kwitter & Henry (1998)

^bOptical line strengths are taken from Kwitter, Henry, & Milingo (2003), while UV

line strengths are taken from Henry, Kwitter, & Howard (1996)

^cOptical line strengths are taken from Milingo, Kwitter, & Henry (2002) and are averages of positions A and B; UV line strengths are taken from Henry, Kwitter, & Bates (2000)

^dAll observed abundances except for carbon are taken from Table 1 of this paper; observed carbon abundances are taken from Henry, Kwitter, & Bates (2000); observed electron densities are taken from same sources as line strengths.

^eMéndez, Kudritzki, & Herrero (1992)

^fStasińska, Górny, & Tylenda (1997)

^gCahn, Kaler, & Stanghellini (1992)

Table 6. S⁺³ Abundance Comparisons

Object	S ⁺³ /H ⁺ (ICF)	S ⁺³ /H ⁺ (IR)	ICF/IR	Reference ^a
DdDm1	3.16E-7	2.3E-7	1.4	1,7
H4-1	2.18E-8	≤3.8E-7	≥0.057	3,7
Hb 12	4.03E-7	3.69E-8	11	2,2
IC3568	4.12E-7	1.18E-6	0.35	1,6
IC4593	7.08E-7	9.88E-7	0.72	1,6
NGC 3918	8.34E-7	2.70E-6	0.31	2,2
NGC 5882	4.00E-6	4.44E-6	0.90	2,2
NGC 6210	2.21E-6	3.48E-6	0.64	1,6
NGC 6567	7.03E-7	2.34E-6	0.30	2,2
NGC 6572	2.11E-6	6.36E-7	3.3	5,6
NGC 6578	4.28E-6	5.98E-6	0.72	2,2
NGC 6884	2.87E-6	3.07E-6	0.93	5,6
NGC 7027	1.96E-6	2.27E-6	0.86	4,6
NGC 7662	3.20E-6	2.74E-6	1.2	2,2

^aThe first number refers to the source for value in column 2, the second number likewise for column 3. 1=Table 8a, this paper; 2=Table 4a, Paper III, where these values have been scaled by 0.75 (6.42/8.54) to reflect recent changes in [S IV] collision strengths published by Tayal (2000); 3=Table 4b, Paper III; 4=Table 4c, Paper III; 5=Table 5c, Paper I; 6=Dinerstein (1980b; these values were updated according to the procedure described in Appendix B); 7=Dinerstein et al. (2003).

Table 7. Abundance Gradients: Fit Parameters

Quantity	Intercept	Slope (dex kpc ⁻¹)	Corr. Coef.	Number	Comp. Slope ^a	[X/H] _{8.5} ^b
12+log(O/H)	8.97±.069	-0.037±.008	-0.45	79	-0.058±.007	-0.08
12+log(Ne/H)	8.37±.11	-0.044±.014	-0.35	77	-0.036±.010	-0.06
12+log(S/H)	7.05±.080	-0.048±.0098	-0.48	81	-0.077±.011	-0.56
12+log(Cl/H)	5.45±.11	-0.045±.013	-0.36	74	-0.070±.010	-0.21
12+log(Ar/H)	6.58±.079	-0.030±.010	-0.34	77	-0.051±.010	-0.19

^aValues quoted directly from Maciel & Quireza (1999) for O, Ne, S, and Ar, and from Maciel & Chiappini (1994) for Cl.

^b $\log(X/H)_{8.5} - \log(X/H)_{\odot}$, the logarithmic offset from the solar value at 8.5 kpc galactocentric distance, where the sources for solar values are discussed in the text.

Table 8A. Ionic Abundances, Temperatures, & Densities

Parameter	DdDm1 ^a	IC418 ^b	IC3568 ^a	IC4593 ^a	NGC6720 ^a	NGC6826 ^{a,e}	NGC7009 ^{a,e}	NGC7293 ^{c,e}	NGC2392 ^{b,d}	NGC6210 ^a
He ⁺ /H ⁺	0.10	6.93E-02	0.12	0.10	7.52E-02	0.11	0.10	0.13	4.20E-02	0.11
He ⁺² /H ⁺	1.01E-03	5.76E-04	4.03E-02	...	1.08E-02	2.94E-03	3.33E-02	1.08E-03
ICF(He)	1.00	1.00	1.00	1.00	1.00	1.00	1.00	1.00	1.00	1.00
O ^o /H ⁺	2.79E-06	7.45E-06	1.91E-05	...	4.63E-07	9.83E-05	3.55E-07	6.83E-06
O ⁺ /H ⁺	3.78E-05	6.21E-05	1.74E-05	8.81E-05	9.97E-05	2.67E-05	7.54E-06	3.79E-04	3.50E-05	2.80E-05
O ⁺² /H ⁺	1.00E-04	7.66E-05	3.57E-04	4.08E-04	3.98E-04	3.90E-04	5.03E-04	2.52E-04	1.74E-04	4.88E-04
ICF(O)	1.00	1.00	1.01	1.01	1.54	1.00	1.10	1.02	1.79	1.01
N ⁺ /H ⁺	7.84E-06	3.69E-05	8.18E-07	4.98E-06	3.49E-05	3.18E-06	3.16E-06	1.36E-04	1.06E-05	6.17E-06
ICF(N)	3.65	2.23	21.63	5.66	7.66	15.62	74.65	1.70	10.71	18.58
Ne ⁺² /H ⁺	1.71E-05	4.16E-06	6.77E-05	7.40E-05	1.08E-04	7.90E-05	1.17E-04	1.65E-04	4.97E-05	1.23E-04
ICF(Ne)	1.38	1.81	1.06	1.22	1.92	1.07	1.12	2.56	2.15	1.07
S ⁺ /H ⁺	2.37E-07	3.05E-07	1.35E-08	9.11E-08	6.73E-07	4.87E-08	1.37E-07	5.33E-07	2.67E-07	2.92E-07
S ⁺² /H ⁺ _{NIR}	1.87E-06	6.53E-06	7.36E-07	3.28E-06	3.09E-06	1.94E-06	3.27E-06	4.76E-06	3.92E-06	4.21E-06
S ⁺² /H ⁺ ₆₃₁₂	2.46E-06	2.30E-06	4.60E-06	7.56E-06	5.69E-06	3.09E-06	3.62E-06	2.88E-07	2.87E-06	3.18E-06
ICF(S)	1.15	1.08	1.55	1.21	1.26	1.43	2.46	1.05	1.33	1.49
Cl ⁺² /H ⁺	2.13E-08	...	3.25E-08	9.09E-08	1.18E-07	8.51E-08	9.01E-08	0.	0.	8.44E-08
Cl ⁺³ /H ⁺	4.21E-08	...	7.40E-08	5.33E-08
ICF(Cl)	1.00	1.00	1.01	1.01	1.54	1.00	1.10	1.02	1.79	1.01
Ar ⁺² /H ⁺	5.16E-07	1.11E-06	6.54E-07	1.51E-06	1.99E-06	1.35E-06	1.56E-06	3.13E-06	8.23E-07	1.30E-06
Ar ⁺³ /H ⁺
ICF(Ar)	1.06	1.22	1.77	1.07	1.12	...	1.98	1.07
T _{O3} (K)	11700	8500	10400	8100	10500	8900	9500	9100	11900	9400
T _{N2} (K)	11400	10700	6700	7300	9400	8700	10200	8500	11400	10200
T _{O2} (K)	10100	17100	8800	6800	5800	6700	10600	8600	6800	10100
T _{S2} (K)	7900	8700	...	(101000)	12900	(117400)	13900	13600	...	9200
T _{S3} (K)	12700	8100	10300	9000	11400	9900	10600	5100	10400	9500
N _{e,S2} (cm ⁻³)	4000	3300	800	1700	600	1700	4300	100	2000	4100

^aine strengths from which these abundances were derived can be found in Kwitter & Henry (1998)

^bine strengths from which these abundances were derived can be found in Kwitter, Henry, & Bates (2000)

^cine strengths from which these abundances were derived can be found in Henry, Kwitter, & Dufour (1999)

^dValues refer to position D

^eValues refer to position B

Table 8B. Elemental Abundances

Element	DdDM1	IC418	IC3568	IC4593	NGC 6720	NGC 6826	NGC 7009	NGC 7293	NGC 2392	NGC 6210	Sun ^a	Orion ^b
He/H	0.10	0.07	0.12	0.10	0.12	0.11	0.12	0.13	0.08	0.11	0.10	0.10
O/H ($\times 10^4$)	1.38	1.39	3.77	4.98	7.64	4.16	5.63	6.47	3.75	5.21	4.90	5.25
N/H ($\times 10^4$)	0.29	0.82	0.18	0.28	2.67	0.50	2.36	2.32	1.14	1.15	0.83	0.60
Ne/H ($\times 10^4$)	0.23	0.08	0.72	0.91	2.08	0.84	1.31	4.23	1.07	1.32	1.20	0.78
S/H ($\times 10^5$)	0.24	0.74	0.12	0.41	0.48	0.28	0.84	0.55	0.56	0.67	1.58	1.48
Cl/H ($\times 10^7$)	0.21	...	0.33	0.91	2.46	0.85	1.81	1.39	1.91	2.14
Ar/H ($\times 10^6$)	0.52	1.11	1.07	1.84	4.29	1.51	2.64	3.13	1.63	1.75	2.51	3.09
N/O	0.21	0.59	0.05	0.06	0.35	0.12	0.42	0.36	0.30	0.22	0.16	0.11
Ne/O	0.17	0.05	0.19	0.18	0.27	0.20	0.23	0.65	0.28	0.25	0.25	0.15
S/O ($\times 10^1$)	0.18	0.53	0.03	0.08	0.06	0.07	0.15	0.09	0.15	0.13	0.32	0.28
Cl/O ($\times 10^3$)	0.15	...	0.09	0.18	0.32	0.20	0.32	0.27	0.39	0.41
Ar/O ($\times 10^2$)	0.37	0.80	0.28	0.37	0.56	0.36	0.47	0.48	0.43	0.34	0.51	0.59

^aGrevesse & Sauval (1998; S, Cl, meteoritic; Ne, Ar, photospheric); O abundance from Allende Priete, Lambert, & Asplund 2001

^bEsteban et al. (1998), Table 19, gas + dust

REFERENCES

- Afflerbach, A., Churchwell, E., & Werner, M.W. 1997, *ApJ*, 478, 190
- Allende Prieto, C., Lambert, D.L., & Asplund, M. 2001, *ApJ*, 556, L63
- Aller, L.H., & Czyzak, S.J. 1983, *ApJS*, 51, 211
- Aller, L.H., & Keyes, C.D. 1987, *ApJS*, 65, 405
- Andrievsky, S.M., Kovtyukh, V.V., Luck, R.E., Lépine, J.R.D., Bersier, D., Maciel, W.J., Barbuy, B., Klochkova, V.G., Panchuk, V.E., & Karpishek, R.U. 2002a, *A&A*, 381, 32
- Andrievsky, S.M., Bersier, D., Kovtyukh, V.V., Luck, R.E., Maciel, W.J., Lépine, J.R.D., & Beletsky, Yu. V. 2002b, *A&A*, 384, 140
- Andrievsky, S. M.; Kovtyukh, V. V.; Luck, R. E.; Lpine, J. R. D.; Maciel, W. J.; Beletsky, Yu. V. 2002c, *A&A*, 392, 491
- Barker, T. 1978a, *ApJ*, 220, 193
- Barker, T. 1978b, *ApJ*, 221, 145
- Barker, T. 1980, *ApJ*, 237, 482
- Barker, T. 1983, *ApJ*, 270, 641
- Barker, T., & Cudworth, K.M. 1984, *ApJ*, 278, 610
- Beck, S.C., Lacy, J.H., Townes, C.H., Aller, L.H., Geballe, T.R., & Baas, F. 1981, *ApJ*, 249, 592
- Cahn, J. H., Kaler, J. B., & Stanghellini, L. 1992, *A&AS*, 94, 399
- Costa, R.D.D., Chiappini, C., Maciel, W.J., & de Freitas Pacheco, J.A. 1996, *A&AS*, 116, 249
- Deharveng, L., Peña, M., Caplan, J., & Costero, R. 2000, *MNRAS*, 311, 329
- Dennefeld, M., & Stasińska, G. 1983, *A&A*, 118, 234
- Dinerstein, H.L. 1980a, Ph.D. thesis, Univ. California, Santa Cruz
- Dinerstein, H.L. 1980b, *ApJ*, 237, 486
- Dinerstein, H.L., Richter, M.J., Lacy, J.H., & Sellgren, K. 2003, *AJ*, 125, 265
- Esteban, C., Peimbert, M., Torres-Peimbert, S., & Escalante, V. 1998, *MNRAS*, 295, 401
- Ferland, G.J. 1996, *Hazy, A Brief Introduction to Cloudy* (Univ. Kentucky Internal Rep.)
- de Freitas Pacheco, J.A. 1993, *ApJ*, 403, 673

- de Freitas Pacheco, J.A., Maciel, W.J., Costa, R.D.D., & Barbuy, B. 1991, *A&A*, 250, 159
- de Freitas Pacheco, J.A., Maciel, W.J., & Costa, R.D.D. 1992, *A&A*, 261, 579
- de Freitas Pacheco, J.A., Costa, R.D.D., & Maciel, W.J. 1993a, *A&A*, 279, 567
- de Freitas Pacheco, J.A., Barbuy, B., Costa, R.D.D., & Idiart, T.E.P. 1993b, *A&A*, 271, 429
- French, H. 1981, *ApJ*, 246, 434
- Garnett, D.R. 1989, *ApJ*, 345, 282
- Garnett, D.R. 1992, *AJ*, 103, 1330
- Garnett, D.R., & Lacy, J.H. 1993, *ApJ*, 419, L93
- Grevesse, N., & Sauval, A.J. 1998, *Space Sci. Rev.*, 85 161
- Gummersbach, C.A., Kaufer, A., Schäffer, D.R., Szeifert, T., & Wolf, B. 1998, *A&A*, 338, 881
- Gutiérrez-Moreno, A., & Moreno, H. 1988, *PASP*, 100, 1497
- Hawley, S.A., & Miller, J.S. 1978, *ApJ*, 220, 609
- Henry, R.B.C. 1989, *MNRAS*, 241, 453
- Henry, R.B.C., Kwitter, K.B., & Bates, J.A. 2000, *ApJ*, 531, 928
- Henry, R.B.C., Kwitter, K.B., & Dufour, R.J. 1999, *ApJ*, 517, 782
- Henry, R.B.C., Kwitter, K.B., & Howard, J.W. 1996, *ApJ*, 458, 215
- Holweger, H. 2001, Joint SOHO/ACE workshop "Solar and Galactic Composition", Robert F. Wimmer-Schweingruber, ed, *AIP Conf. Proc.*, 598, p.23
- Howard, J.W., Henry, R.B.C., & McCartney, S. 1997, *MNRAS*, 284, 465
- Kennicutt, R.C., Bresolin, F., & Garnett, D.R. 2003, *ApJ*, 591, 801 (KBG)
- Kingsburgh, R.L., & Barlow, M.J. 1994, *MNRAS*, 271, 257 (KB)
- Kwitter, K.B., & Henry, R.B.C 1998, *ApJ*, 493, 247
- Kwitter, K.B., & Henry, R.B.C. 2001, *ApJ*, 562, 804 (Paper I)
- Kwitter, K.B., Henry, R.B.C., & Milingo, J.B. 2003, *PASP*, 115, 80 (Paper III)
- Lester, D.F., Dinerstein, H.L., & Rank, D.M. 1979, *ApJ*, 229, 981
- Luridiana, V., Esteban, C., Peimbert, M., & Peimbert, A. 2002, *Rev. Mex. A. Af.*, 38, 97

- Maciel, W.J. 1984, *A&AS*, 55, 253
- Maciel, W.J., & Chiappini, C. 1994, *Astroph. Space Sci.*, 219, 231
- Maciel, W.J., & Köppen, J. 1994, *A&A*, 282, 436
- Maciel, W.J., & Quireza, C. 1999, *A&A*, 345, 629
- McWilliam, A. 1997, *ARA&A*, 35, 503
- Méndez, R. H., Kudritzki, R. P., & Herrero, A. 1992, *A&A*, 260, 329
- Milingo, J.B., Kwitter, K.B., Henry, R.B.C., & Cohen, R.E. 2002, *ApJS*, 138, 279 (Paper IIA)
- Milingo, J.B., Henry, R.B.C., & Kwitter, K.B. 2002, *ApJS*, 138, 285 (Paper IIB)
- Nomoto, K., Iwamoto, K., Nakasato, N., Thielemann, F.-K., Brachwitz, F., Tsujimoto, T., Kubo, Y., & Kishimoto, N. 1997, *Nucl. Phys. A*, 621, 467c
- Pagel, B.E.J. 1997, *Nucleosynthesis and Chemical Evolution of Galaxies*, (Cambridge: Cambridge University Press), Chapter 5
- Peimbert, M. 1978, in *Planetary Nebulae*, IAU Symp. 76, ed., Y. Terzian, (Dordrecht: Reidel), p. 215
- Peimbert, M., & Costero, R. 1969, *Bol. Obs. Tonantzintla y Tacubaya*, 5, 3
- Peimbert, M., Torres-Peimbert, S., & Ruiz, M.T. 1992, *Rev. Mex. A. Af.*, 24, 155
- Péquignot, D., Walsh, J.R., Zijlstra, A.A., & Dudziak, G. 2000, *A&A*, 361, L1
- Peña, M., Torres-Peimbert, S., & Ruiz, M.T. 1991, *PASP*, 103, 865
- Rodríguez, M. 1999, *A&A*, 351, 1075
- Rolleston, W.R.J., Smartt, S.J., Dufton, P.L., & Rayns, R.S.I 2000, *A&A*, 363, 537
- Sabbadin, F. 1986, *A&AS*, 64, 579
- Savage, B.D., & Sembach 1996, *ARA&A*, 34, 279
- Shaver, P.A., McGee, R.X., Newton, L.M., Danks, A.C., & Pottasch, S.R. 1983, *MNRAS*, 204, 53
- Snedden, C., & Cowan, J.J. 2003, *Science*, 299, 70
- Stasińska, G., S.K. Górný, & Tylenda, R. 1997, *A&A*, 327, 736
- Tayal, S.S. 2000, *ApJ*, 530, 1091
- Torres-Peimbert, S., & Peimbert, M. 1979, *Rev. Mex. A. Af.*, 4, 341

- Torres-Peimbert, S. Peimbert, M., Peña, M. 1990, A&A, 233, 540
- Trundle, C., Dufton, P.L., Lennon, D.J., Smartt, S.J., & Urbaneja, M.A. 2002, A&A, 395, 519
- Truran, J.W., Cowan, J.J., Pilachowski, C.A., & Sneden, C. 2002, PASP, 114, 1293
- Tsamis, Y.G., Barlow, M.J., Liu, X.-W., Danziger, I.J., & Storey, P.J. 2003, MNRAS, 338, 687
- Twarog, B.A., Ashman, K.M., Anthony-Twarog, B.J. 1997, AJ, 114, 2556
- Vermeij, R., & van der Hulst, J.M. 2002, A&A, 391, 1081
- Vílchez, J.M., & Esteban, C. 1996, MNRAS, 280, 720
- Woosley, S.E., & Weaver, T.A. 1995, ApJS, 101, 181
- Zhang, C.Y. 1995, ApJS, 98, 659

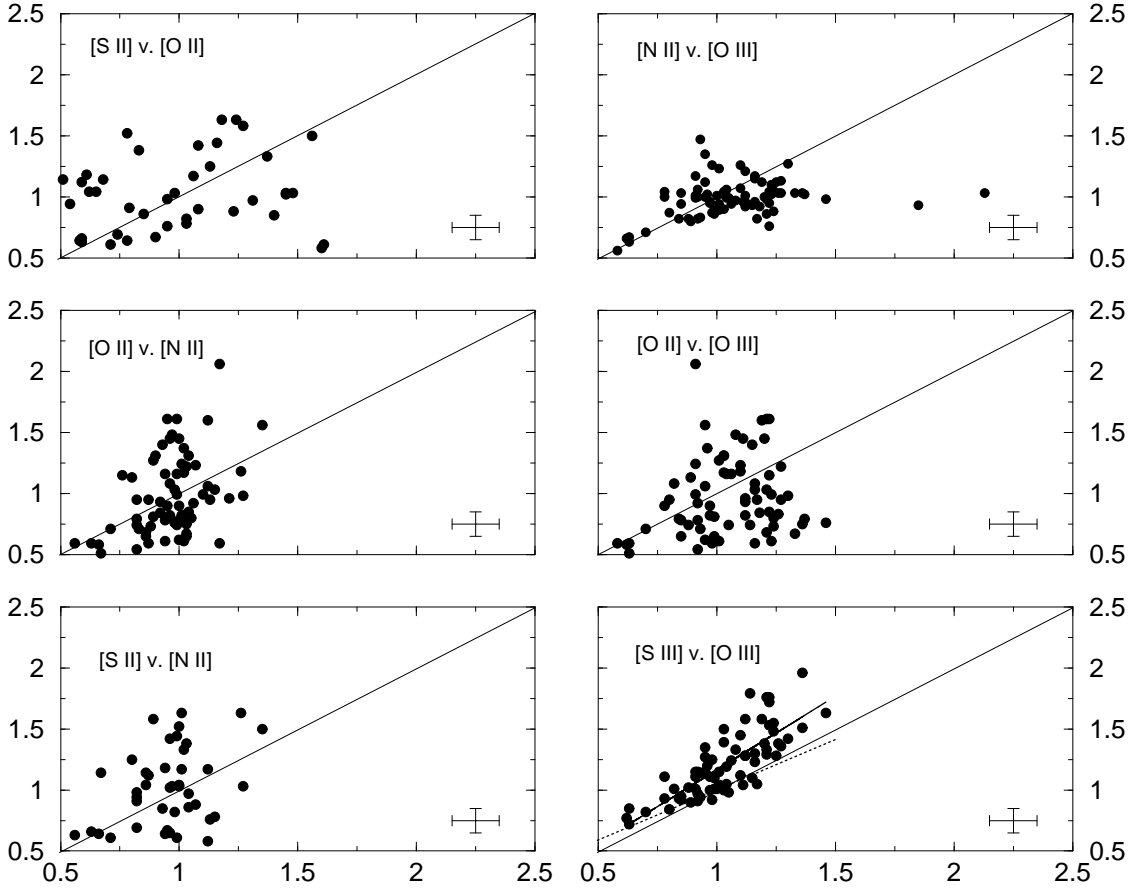


Fig. 1.— Comparisons of five electron temperatures (in units of 10^4K) for our sample objects in various combinations. Each panel is labeled to show the temperatures being plotted, Y v. X. The diagonal lines show the one-to-one correspondence. In the lower right panel, the solid bold line shows our least squares fit to the data (eq. 1), while the dashed line shows the functional form derived by Garnett (1992) in a photoionization model study of H II regions.

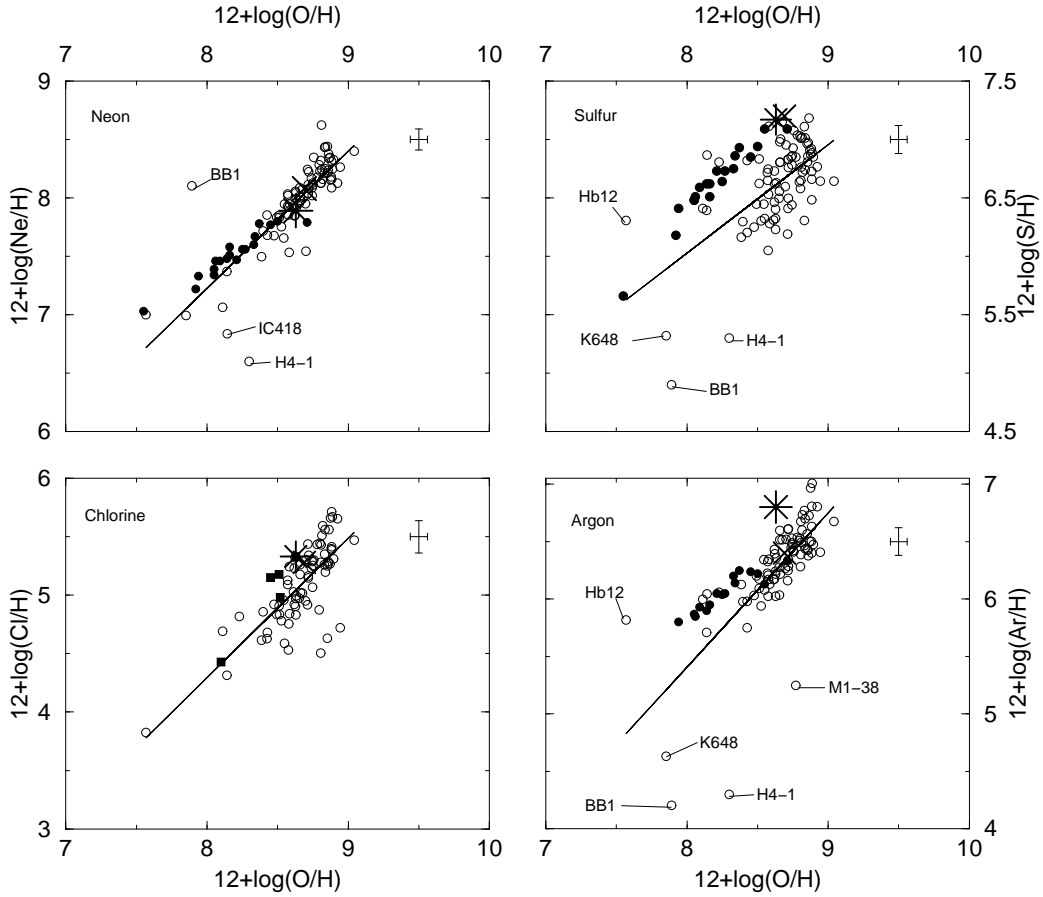


Fig. 2.— Plots of $12+\log(\text{X}/\text{H})$ versus $12+\log(\text{O}/\text{H})$, where X is the element specified in the upper left of each graph. Results are shown for both the PNe in the current sample (open circles) as well as the data for H II regions in M101 as measured by KBG (filled circles), Orion (Esteban et al. 1998; star) and the Sun (Grevesse & Sauval 1998 but with oxygen abundance from Allende Prieto et al. 2001; X). H II region data for Cl are taken from references in Table 3 and are shown as filled squares. Solid, bold lines show least squares fits to our PN data, where the slopes and intercepts for the regressions are provided in Table 4. A representative error bar is shown in each panel. Certain outliers are identified in the figure and discussed in the text.

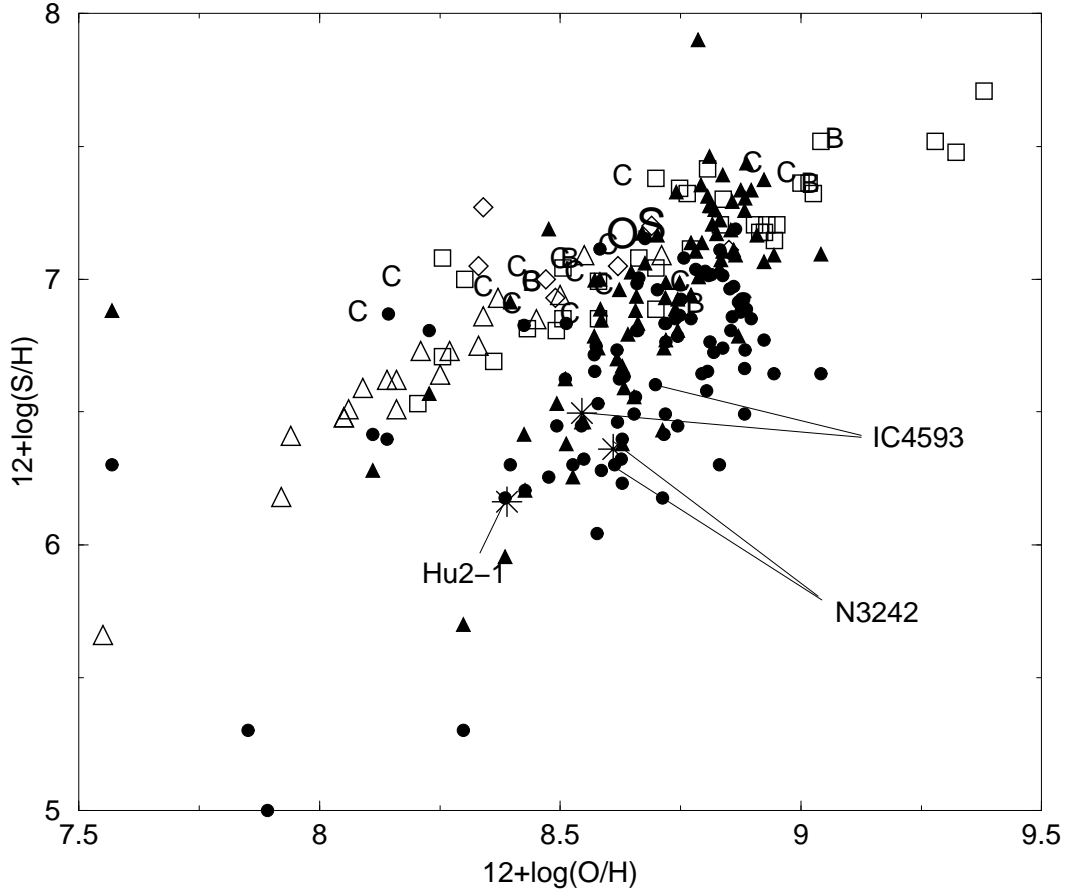


Fig. 3a.— $12+\log(\text{S}/\text{H})$ versus $12+\log(\text{O}/\text{H})$ for PNe from this paper (filled symbols) and H II regions from several sources (open symbols). Filled circles show PN results in which S^{+2} results for our sample were derived from the [S III] $\lambda\lambda 9069, 9532$ lines, while filled triangles show analogous results using the [S III] 6312\AA line. H II region abundances are taken from Shaver et al. (1983; open diamonds), Afflerbach, Churchwell, & Werner 1997; open squares), and KBG (open triangles). Also shown are results for the Orion Nebula from Esteban et al. (1998; O), the Sun (Grevesse & Sauval 1998 for the S abundance, Allende Prieto et al. 2001 for the O abundance; S), Cepheids from Andrievsky et al. (2002a,b,c; C) and for B giants (Trundle et al. 2002; B). Model-predicted values for Hu2-1, IC4593, and NGC 3242 are shown with stars (see text for explanation). Uncertainties for each data set are [in the form $\pm d\log(\text{S}/\text{H}), \pm d\log(\text{O}/\text{H})$]: Shaver et al., 0.06,0.04; Afflerbach et al., 0.22,0.35; KBG, 0.11,0.07; this paper, 0.12,0.06.

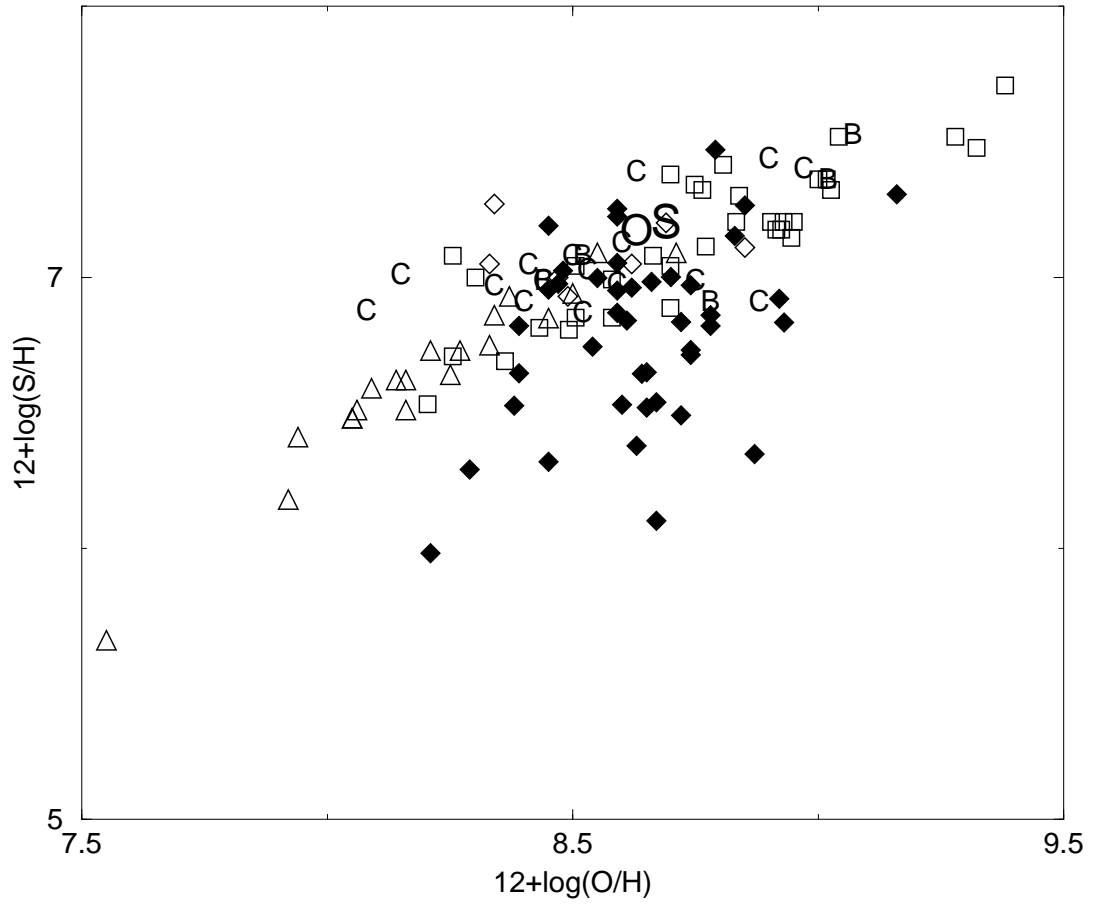


Fig. 3b.— Same as 3a but showing the KB PN sample as filled diamonds.

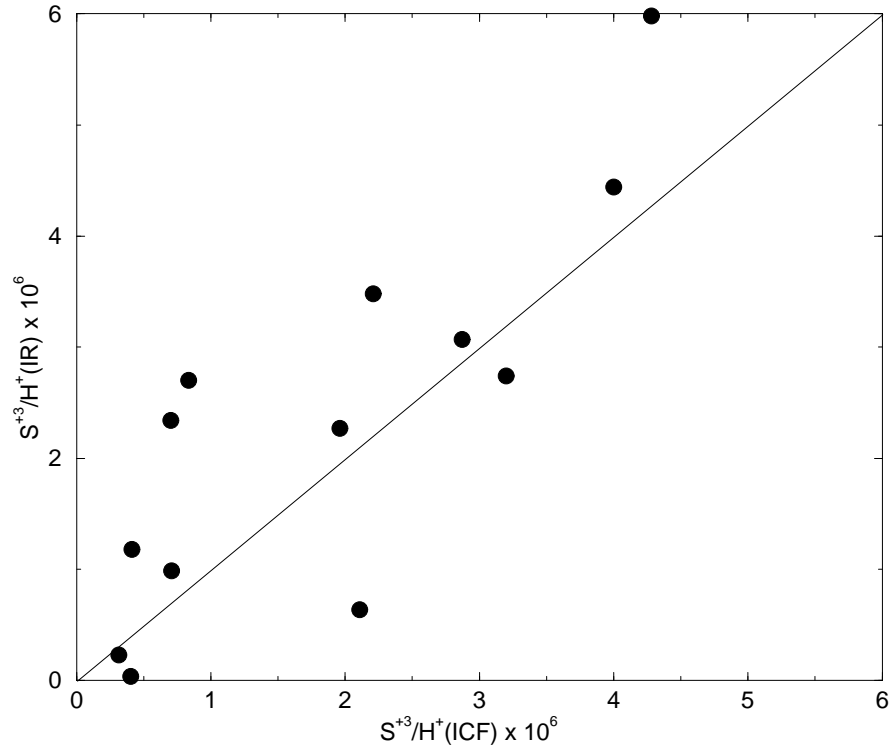


Fig. 4.— S^{+3}/H^+ determined from direct IR measurements of [S IV] $10.5\mu\text{m}$ versus the same parameter inferred from our ICF. Both sets of numbers are taken directly from columns 3 and 2 in Table 6, respectively. The diagonal line shows the one-to-one correspondence.

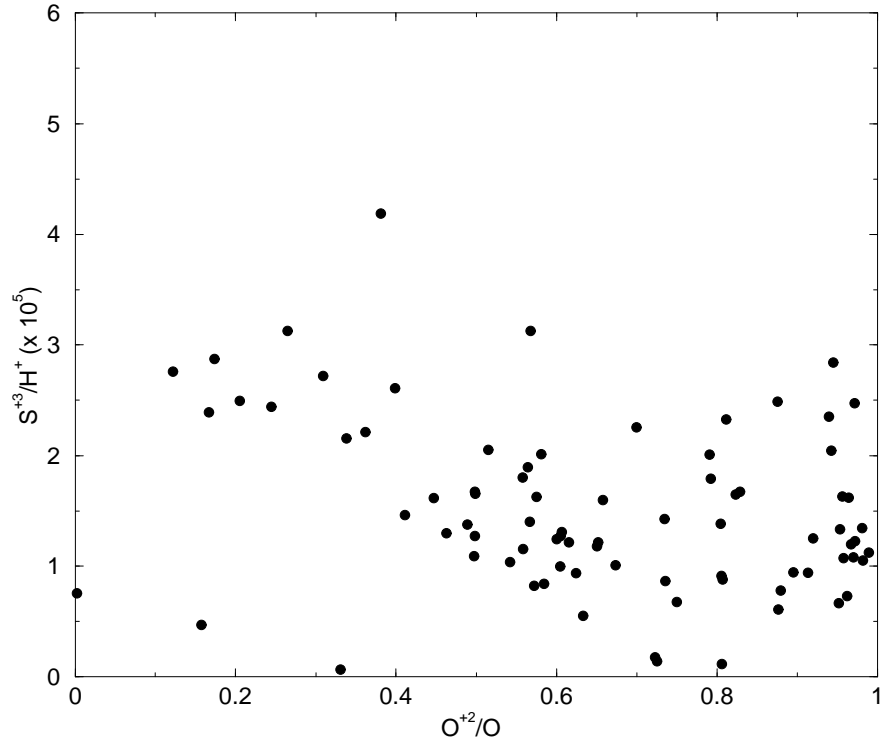


Fig. 5.— Predicted values of the sulfur deficit (see text) in units of $S^{+3}/H^+ (x 10^5)$ versus observed results for O^{+2}/O for members of our PN sample.

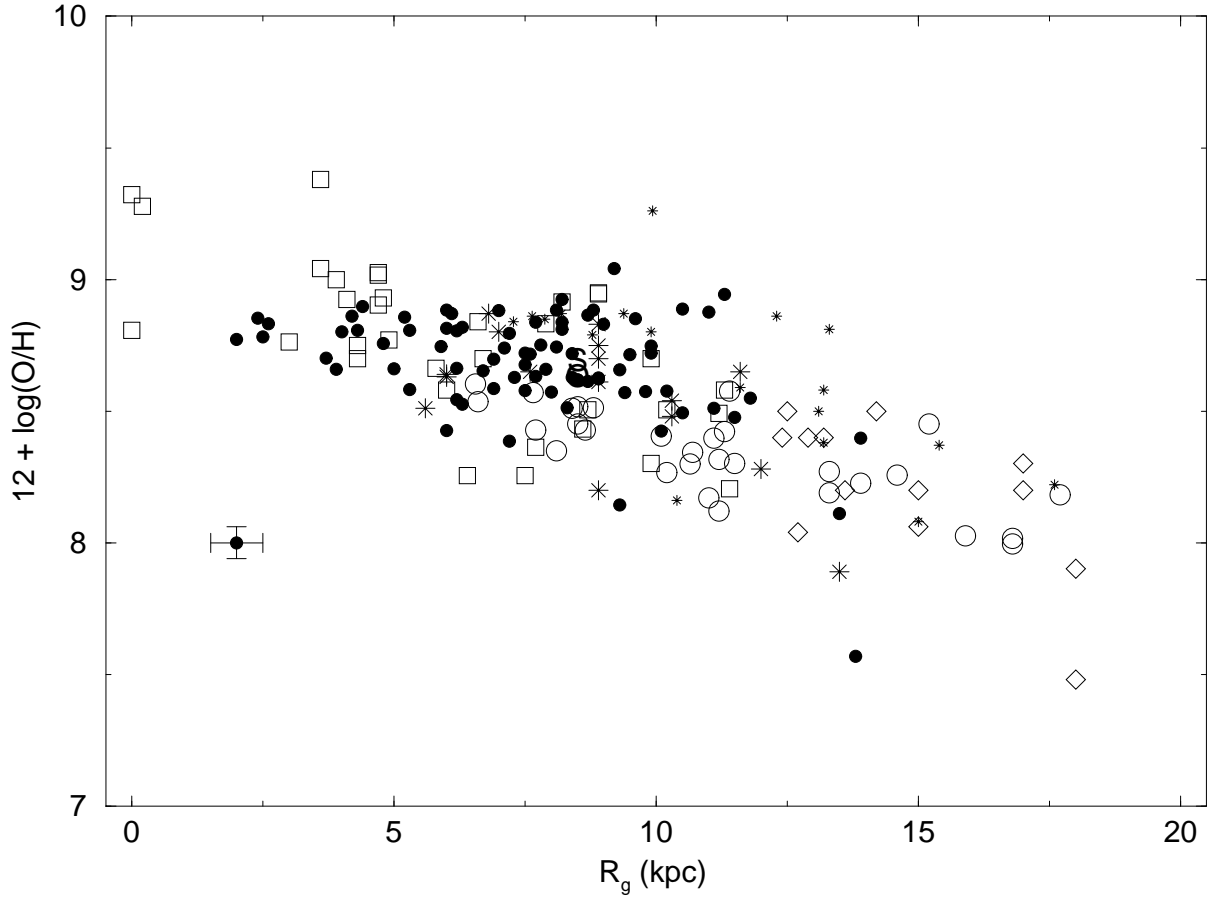


Fig. 6a.— $12 + \log(\text{O}/\text{H})$ versus galactocentric distance in kiloparsecs. Our abundance results are shown with filled circles. H II region abundances as determined by Afflerbach, Churchwell, & Werner (1997; open boxes), Deharveng et al. (2000; open circles) and Vílchez & Esteban (1996; open diamonds) are shown for comparison, as are B main sequence stellar data from Gummersbach et al. (1998; large stars) and Rolleston et al. (2000; small stars).

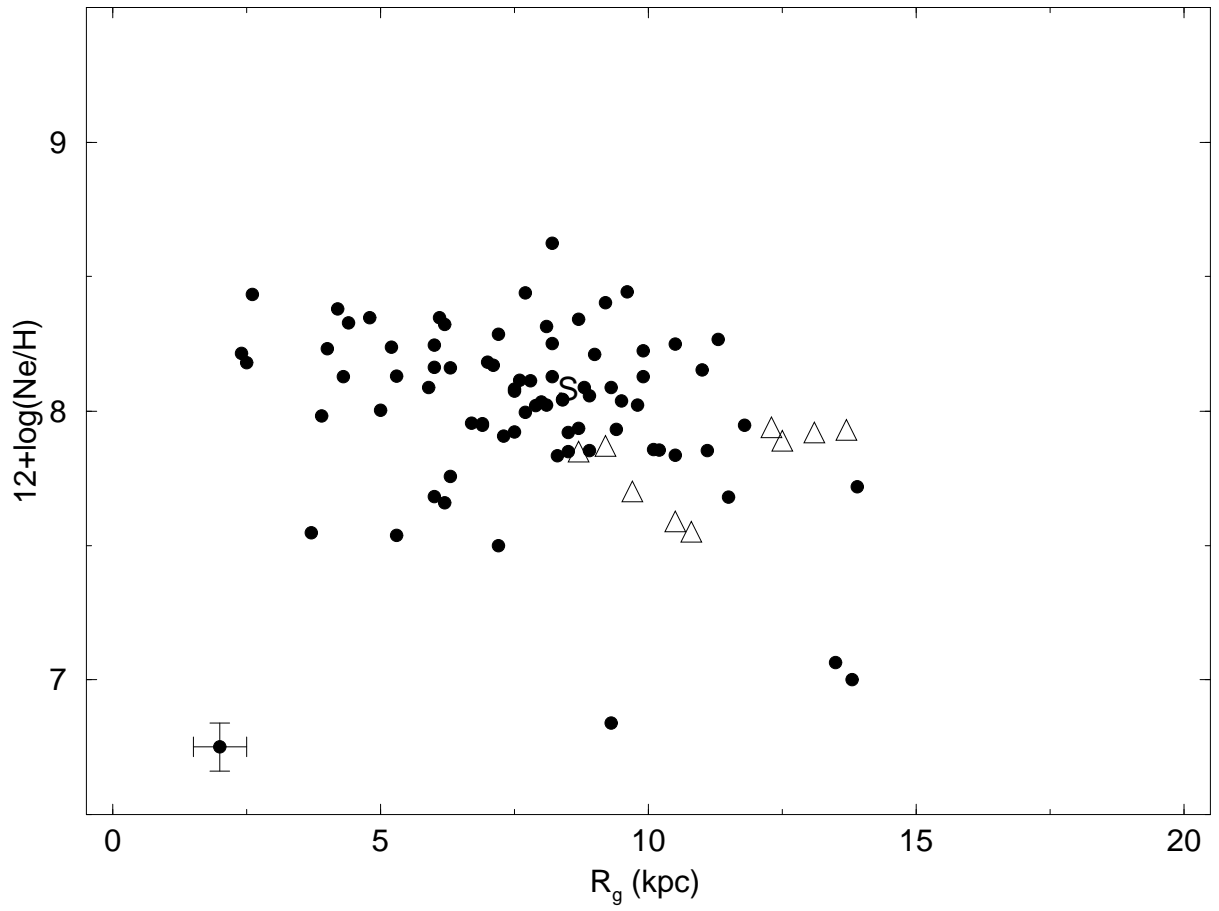


Fig. 6b.— Same as Fig. 6a but for neon. Data from Shaver et al. (1983; up triangles) are shown for comparison.

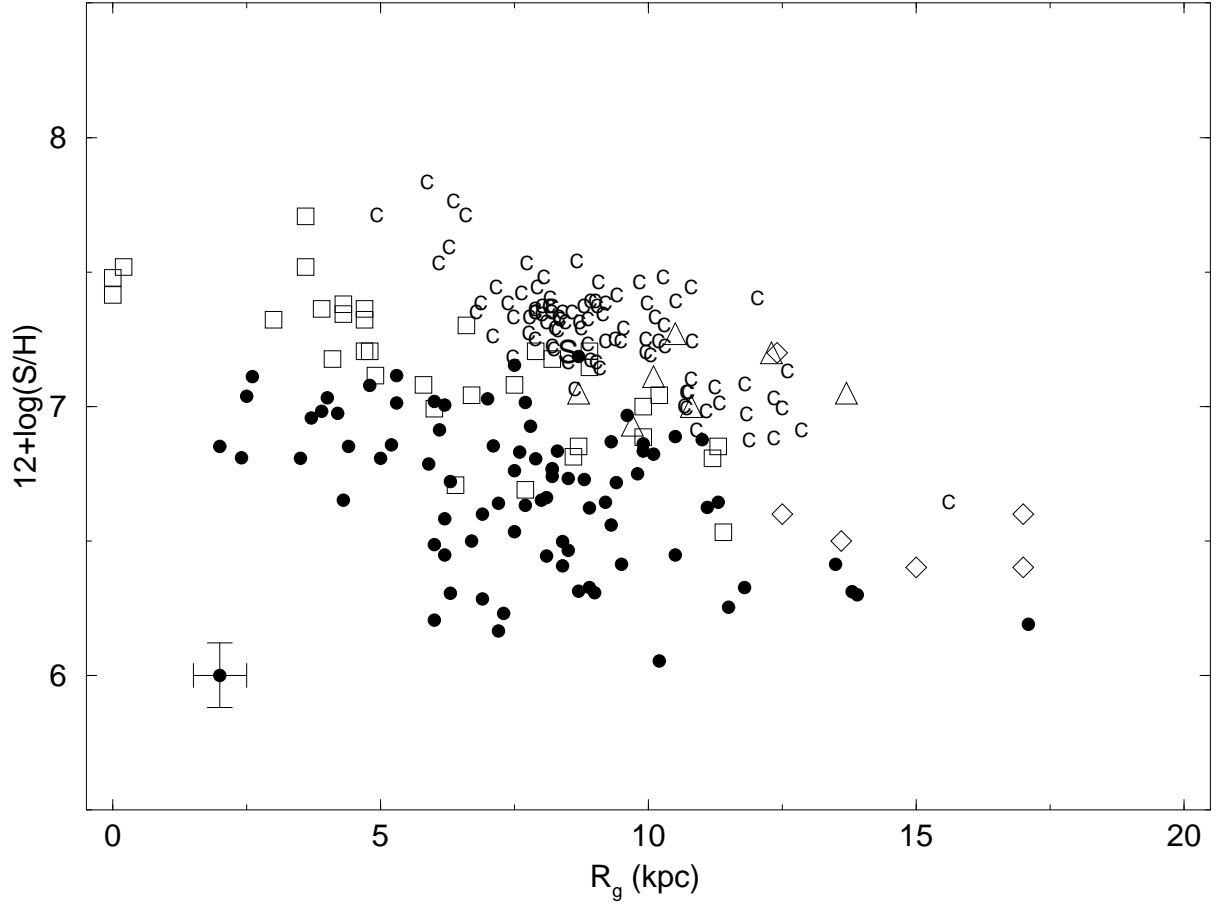


Fig. 6c.— Same as Fig. 6a but for sulfur. Data from Shaver et al. (1983; up triangles), Afflerbach, Churchwell, & Werner (1997; open boxes), and Vílchez & Esteban (1996; open diamonds) for H II regions as well as data for 100 Cepheids from Andrievsky et al. (2002a,b,c; C) are shown for comparison.

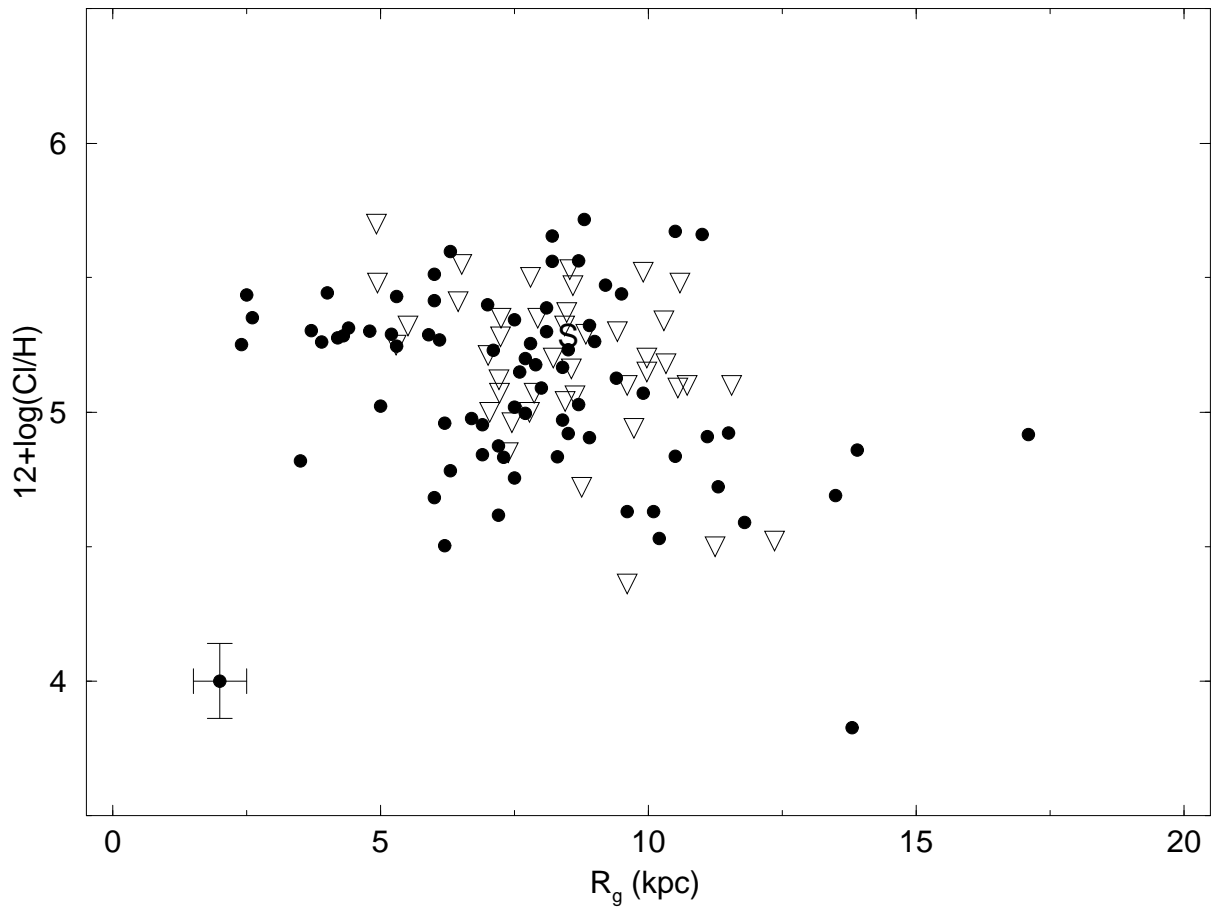


Fig. 6d.— Same as Fig. 6a but for chlorine. PN data from Maciel & Chiappini (1994; down triangles) are shown for comparison.

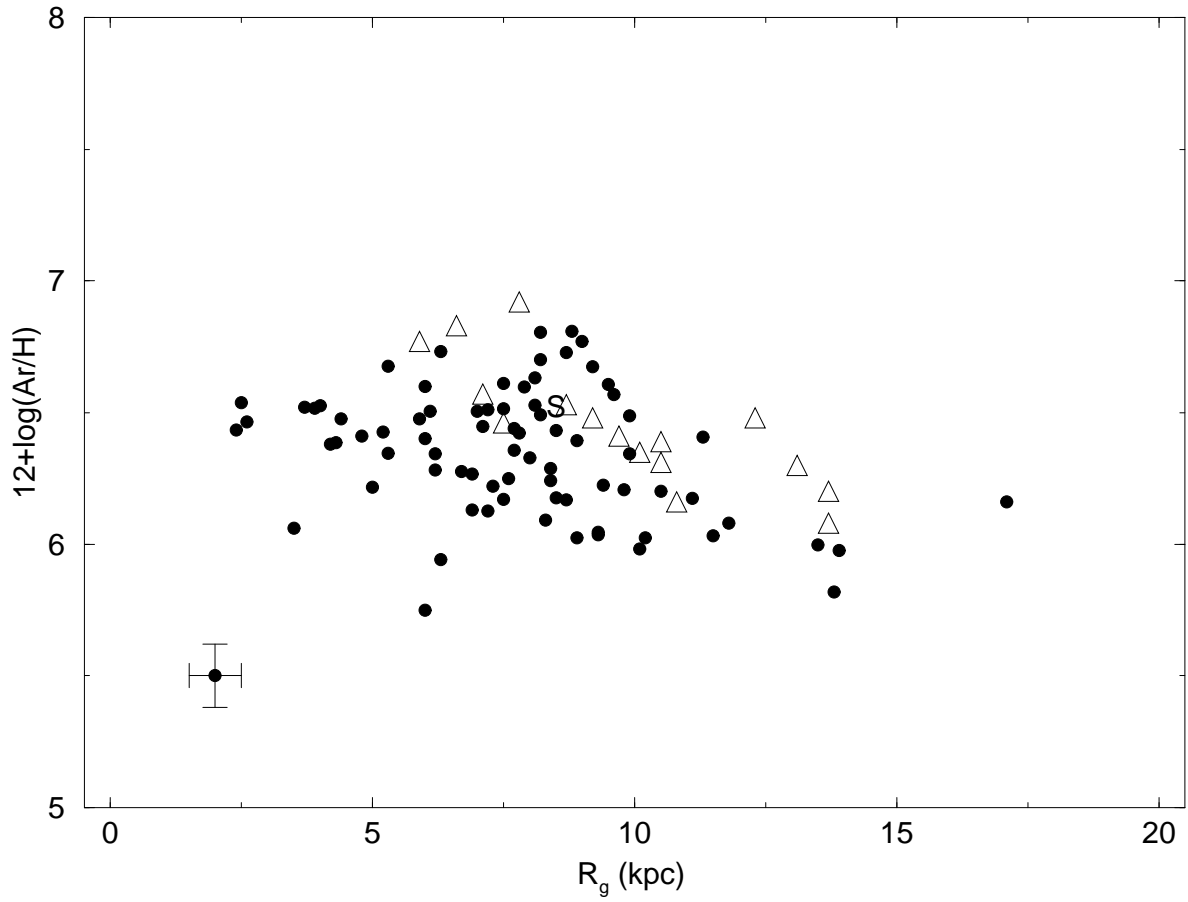


Fig. 6e.— Same as Fig. 6a but for argon. Data from Shaver et al. (1983; up triangles) for H II regions are shown for comparison.